MARINE GEORESOURCES & GEOTECHNOLOGY
https://doi.org/10.1080/1064119X.2025.2507809

An economic block model-based framework to determine design requirements for ferromanganese crust mining systems

Raoul Schmitt[a], Maxime Lesage[b] and Steinar Løve Ellefmo[a]

[a]Department of Geosciences, Norwegian University of Science and Technology (NTNU), Trondheim, Norway; [b]Green Minerals AS, Oslo, Norway

ABSTRACT

Ferromanganese crust (FMC) deposits are potential targets for commercial deep-sea mining. To guide future mining system design studies and the development of complementary mining equipment, this study introduces a framework that uses economic block models to identify design requirements for FMC mining systems that impact deposit value. The framework is illustrated through a case study of a hypothetical FMC deposit in a prospective region. Results show that mining efficiency has the greatest impact on deposit value, emphasizing that future designs should prioritize maximizing efficiency. System mobility and adaptability to manage steep slopes are also identified as influential design parameters. Economically, FMC mining is characterized as a cobalt-manganese venture.

ARTICLE HISTORY
Received 29 December 2024
Accepted 13 May 2025

KEYWORDS
Deep-sea mining; block model; sensitivity analysis; design parameters; slope angle

1. Introduction

The development of modern society and economic growth rely on mineral raw materials (Dubiński and Koteras 2023). As nations work toward achieving net-zero CO_2 emissions, the demand for critical raw materials, particularly those essential for clean energy technologies, is expected to increase. However, current supply from mining and recycling is unlikely to meet this growing demand within this decade (Cathles and Simon 2024; ETC 2023; IEA 2024a). This possible shortfall requires the investigation of alternative sources, such as marine minerals obtained by deep-sea mining (DSM). Although research on DSM dates back to the 1960s (Sparenberg 2019), no commercial-scale operations exist yet (Miller et al. 2021).

DSM projects are likely to target polymetallic nodules (PMN), seafloor massive sulfides (SMS), and ferromanganese crusts (FMC) (Hein et al. 2013; Miller et al. 2021). It has been argued that commercial-scale DSM could cause unpredictable, long-lasting, and irreversible harm to marine ecosystems (Amon et al. 2022; Howard et al. 2020; Washburn et al. 2019).

Recent DSM developments highlight the growing global interest in DSM (Figure 1). For example, Japan has identified over 200 million metric tons of PMN within its exclusive economic zone (EEZ) and plans to begin trial exploitation by 2026 (The Japan Times 2024). In 2022, the Cook Islands issued three exploration licenses for seabed minerals (SBMA 2023), while Norway suspended a licensing round that would have granted first commercial exploration licenses on its extended continental shelf in 2025 (Fouche and Adomaitis 2024). The Metals Company (TMC) conducted a first integrated PMN pilot mining trial in the Clarion Clipperton Zone (CCZ) since the 1970s and successfully produced cobalt and nickel sulfates, and manganese silicate (TMC 2022, 2024a, 2024b, 2025). In contrast, Nautilus Minerals' Solwara-1 SMS project in Papua New Guinea, which aimed to extract 1.35 million tons of dry ore annually, failed due to bankruptcy (SRK Consulting 2010; Stutt 2019). Despite the significant advancements in mining systems for PMN and SMS, no commercial-scale systems exist for FMC, with only two pilot-scale mining tests conducted so far (Orita et al. 2022; Xie, Chen, et al. 2022) (Figure 1), indicating a lack of documented FMC mining systems (CMS).

Marine mineral resources such as PMN and SMS are generally reported according to international guidelines developed for land-based mining projects (Lipton, Nimmo, and Parianos 2016, Lipton, Gleeson, and Munro 2018; Madureira et al. 2016; Parianos, Lipton, and Nimmo 2021), which, by extension, may be applicable to future FMC mining. To demonstrate a mining project's technical and economic viability, companies typically conduct a feasibility study that includes a mineral reserve estimate. Such estimates are derived by applying modifying factors—including mining, metallurgical, economic, and environmental considerations—to mineral resources identified during exploration (CRIRSCO 2024; Hartman and Mutmansky 2002). However, the lack of precedents and knowledge about the CMS likely

CONTACT Raoul Schmitt raoul.schmitt@ntnu.no Department of Geosciences, Norwegian University of Science and Technology (NTNU), S. P. Andersens veg 15a, 7031 Trondheim, Norway

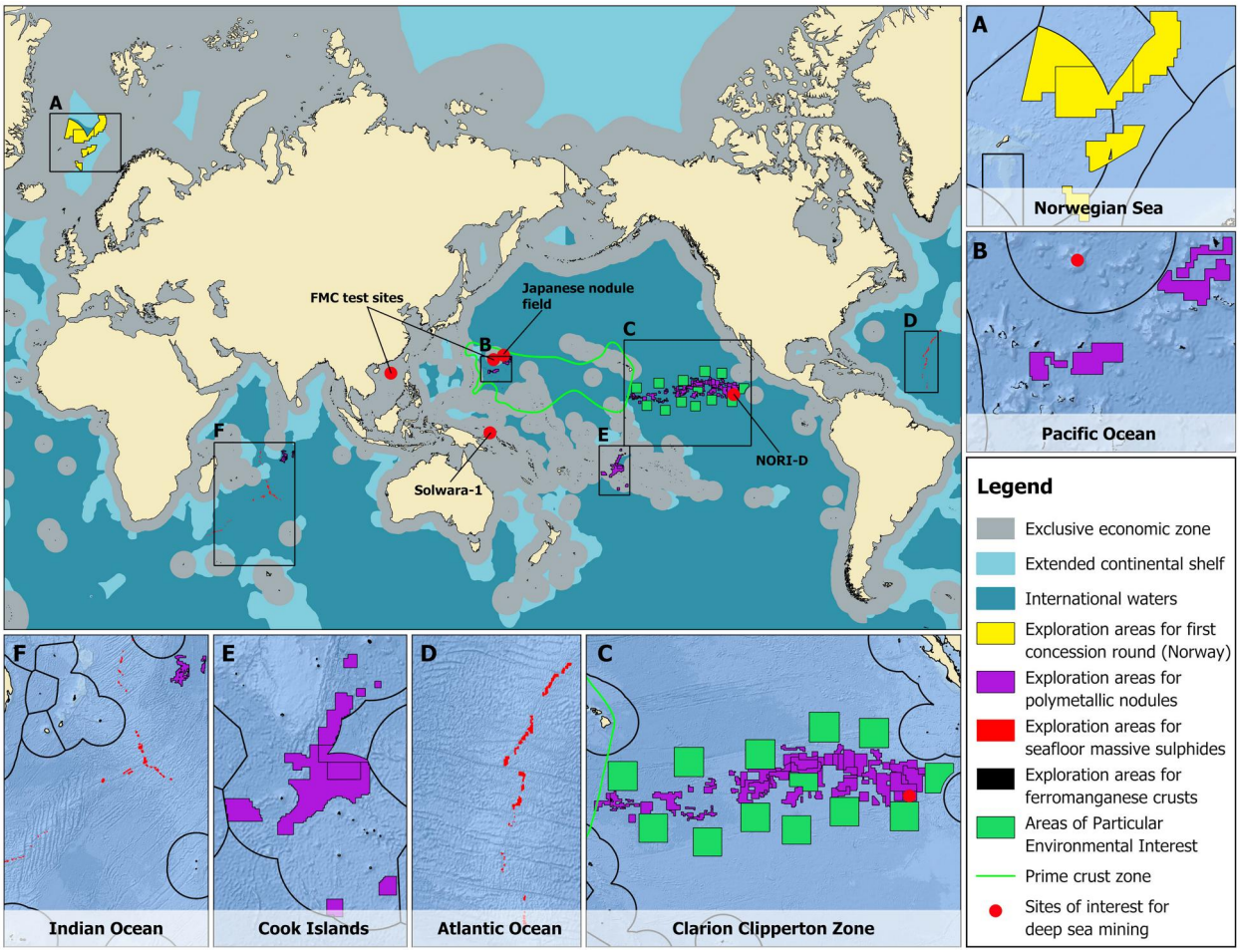

Figure 1. Global map of areas and sites associated with deep-sea mineral activities. Maritime boundaries are taken from Flanders Marine Institute (2023, 2024). Exploration areas include: international waters (ISA 2024a), the Norwegian-Greenland sea (SODIR 2024), and the Cook Islands (Tay, Browne, and Bertoli 2022). The boundaries of the Prime crust zone were defined by Hein, Conrad, and Dunham (2009). Locations of sites of interest are from different publications (AMC 2021; Machida et al. 2016; Orita et al. 2022; SRK Consulting 2010; Xie, Chen, et al. 2022). Basemap is provided by ESRI (2014).

complicates the application of modifying factors, thereby hindering the demonstration of project viability.

Lesage (2019) emphasized that the cost structure of DSM projects is primarily determined by the mining system employed. Estimating the cost of a CMS involves a design study, which begins by defining the system's initial design requirements (Pahl et al. 2007). To address these requirements, this study presents a framework for identifying the value-generating design requirements of a CMS using an economic block model (EBM). Key considerations include determining mineable slope angles, mining system efficiencies, mobility requirements, and other critical factors. The framework is illustrated through a hypothetical case study of an FMC deposit, demonstrating the potential of integrating EBMs into a structured approach to DSM system design. While hypothetical, the EBM also provides valuable insights into significant economic considerations, such as the role of metallurgical processing, and the broader potential economic benefits of FMC mining. Others have developed EBMs for SMS mining (Ellefmo 2022; Lesage, Juliani, and Ellefmo 2018), where geological block models are combined with a techno-economic framework to estimate block revenues, costs, and block-specific dollar-values. The cumulative value of all blocks in the EBM represents the deposit's undiscounted total value. Here, *deposit* refers to the hypothetical FMC mineralization, while *ore* describes the portion that could potentially be extracted profitably. These terms are descriptive only and do not imply the estimation of mineral resources or reserves. Likewise, *deposit value* does not necessarily reflect the actual economic value of an FMC deposit.

To facilitate the development of a preliminary EBM, the following key limitations and assumptions were made:

1. Mine site location: The potential implications of the site's location are disregarded, and specific transport routes and port locations are not assessed.
2. Ore deposit: A pavement-like FMC is assumed to overlie a uniform substrate, for example, altered basalt. However, in the absence of sample data from the hypothetical mine site, it is not currently possible to distinguish among specific FMC types or among specific substrate types. Correlations between FMC thickness, water depth, and metal grades (Halbach and Manheim 1984; Hodkinson and Cronan 1991;

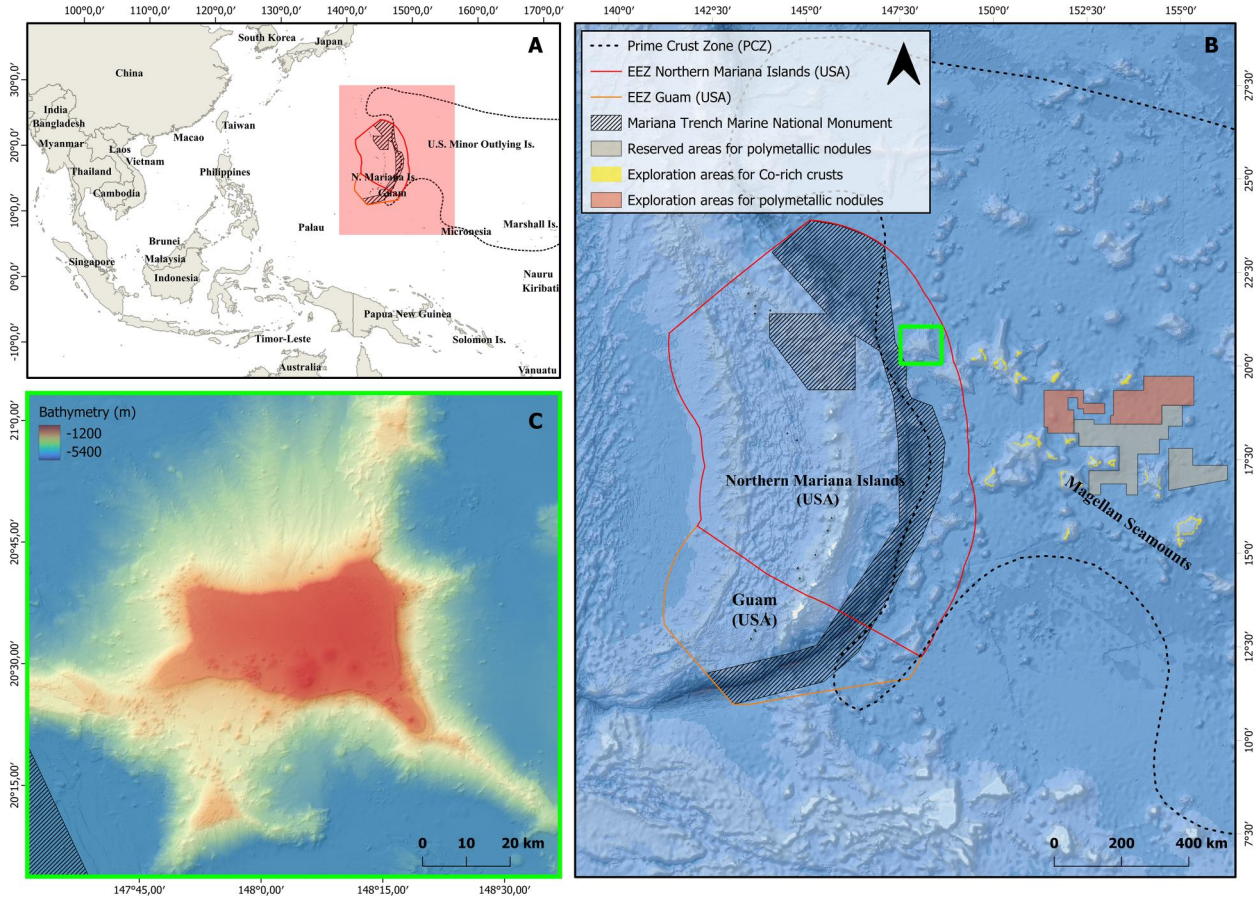

Figure 2. Regional map showing the study area in the Western pacific ocean (A). Fryer guyot's location within the Northern Mariana Islands' EEZ (Flanders Marine Institute 2023) and the PCZ (Hein, Conrad, and Dunham 2009), and east of the mariana trench national monument (UNEP-WCMC & IUCN, 2024). Licenses for exploration areas for FMC and PMN are issued by ISA (ISA 2024a) (B). Bathymetric map of Fryer Guyot (NOAA 2023) (C). Basemap provided by ESRI (2014).

Usui et al. 2017) are not considered, and FMC microtopography (Usui et al. 2017; Yamazaki and Sharma 1998) is disregarded.

3. Mining system configuration: The CMS is informed by existing DSM concepts (e.g., AMC 2021; SRK Consulting 2010).
4. Mineral processing: Metallurgical processing assumes FMC and PMN are mineralogically, chemically, and texturally similar. Metallurgical byproducts and waste management are not considered.
5. Deposit value: The deposit value is calculated based on the extracted value of ore, excluding financial considerations such as discounting, taxes, and royalties.
6. Economies of scale: The analysis does not account for potential economies of scale that may affect costs and efficiencies.
7. Market considerations: Products are sold to established markets without accounting for potential fluctuations in commodity prices.

2. Background

2.1. Geological rationale and mining considerations

Due to the limited publicly available geological data for FMC, Fryer Guyot—a large seamount in the Prime Crust Zone (PCZ) with comprehensive ~100 m × 100 m bathymetric data—was selected as a hypothetical mine site (Figure 2). Much of the research on FMC has focused on the PCZ, considered prospective owing to the presence of thick FMC with high metal content (Halbach, Jahn, and Cherkashov 2017; Hein et al. 2000, Hein, Conrad, and Dunham 2009; Hein et al. 2012; Hein et al. 2013; Hein and Koschinsky 2014; Josso et al. 2023; Mizell et al. 2022; Petersen et al. 2016). The guyot's location within the PCZ supports the assumption of hosting an FMC deposit suitable for multiyear mining. However, only visual documentation of FMC at Fryer Guyot is available (Amon et al. 2022).

Although thick sediment layers on guyot summits may inhibit FMC growth (Hein et al. 2000; Zhao et al. 2020), strong bottom currents along the seamount flanks help keep the flank substrate sediment-free. (Hein, Conrad, and Dunham 2009, Hein et al. 2013). Furthermore, research indicates that FMC precipitate on substrates with slope angles greater than 4° (Du et al. 2020; Yamazaki and Sharma 1998). However, FMC coverage may be discontinuous or even occur beneath sediment layers (Du et al. 2017; Neettiyath et al. 2022; Yamazaki and Sharma 1998). Commercial FMC extraction will likely occur primarily at depths of 800–2500 m, where researchers have identified thick, metal-rich FMC (Halbach et al. 1987; Hein, Conrad,

Table 1. Summary of key aspects related to ferromanganese crusts.

Aspect	Description	References
Occurrence	Occur on ridges, plateaus, seamounts, and other bathymetric highs of all ocean basins. May be present below sediment layers.	Hein (2004); Manheim and Lane-Botswick (1989); Neettiyath et al. (2022); Yamazaki and Sharma (1998)
Formation mechanism	Metal precipitation from seawater onto hard, sediment-free substrates driven by water mixing.	Hein, Conrad, and Dunham (2009, Hein et al. 2013); Hein and Koschinsky (2014); Koschinsky and Halbach (1995)
Appearance	Closely resemble seafloor morphology and form pavements (up to 25 cm thick) or cover boulders of varying size.	Hein et al. (2017); Hino et al. (2024); Usui et al. (2017)
Metals of economic interest and economic importance	Manganese, cobalt, copper, nickel, tellurium, and rare earth elements (REEs), which are considered critical raw materials for clean energy technologies.	European Commission: Directorate-General for Internal Market, Industry, Entrepreneurship and SMEs et al. (2023); Halbach, Jahn, and Cherkashov (2017); Hein et al. (2000, 2013, Hein, Koschinsky, and Kuhn 2020)
Exploration status	Four ISA contracts have been issued in the Pacific Ocean (Korea, China, Japan, Russia)	ISA (2024b)
Mining machines and concepts	Self-propelled crawlers with mechanical cutting devices in combination with vertical lifting systems and support vessels.	Halkyard (1985); Halvorsen (2022); Orita et al. (2022); Xie, Wang, et al. (2022)

and Dunham 2009; Hein et al. 2017). Key aspects related to FMC are summarized in Table 1.

Commercial FMC extraction is likely to result in ore and metal losses at various stages of the DSM value chain, which can be quantified using efficiency factors. Studies on SMS, PMN, and FMC mining have examined various efficiency factors, including ore fragmentation, collection, and transport (AMC 2021; Ellefmo 2022; Goto et al. 2010; Morgan 2006; SRK Consulting 2010; Volkmann and Lehnen 2018; Yamazaki et al. 2002). Together, these factors determine overall mining efficiency. Additionally, ore dilution due to co-extraction of the underlying substrate (e.g., basalt) is likely to negatively impact future FMC mining operations (Cruickshank and Paul 1986; Morgan 2006; Yamazaki et al. 2002). Similar to onshore mining practices (Ebrahimi 2013), a dilution factor for FMC represents the ratio of the wet mass of mined substrate to the total wet mass of extracted material. Regarding FMC mining claims, ISA set a maximum exploration area of 20 km^2 for a "cobalt crust block" (ISA 2012), a block size that Hein (2006) suggested and ISA later adopted.

2.2. Processing route

Since the 1970s, extensive research has been conducted on the metallurgical processing of PMN, typically focusing on recovering three to four metals—Co, Ni, Cu, and sometimes Mn—through hydrometallurgical and pyrometallurgical processes (Agarwal et al. 1976; AMC 2021; Dames & Moore and EIC Corporation 1977; Das and Anand 2017; Fuerstenau and Han 1983; Haynes, Law, and Maeda 1983; Little 1984). Other researchers have explored similar processing routes in their theoretical studies on PMN (Fritz et al. 2023; Kirchain et al. 2019). Although research on FMC processing is limited, PMN processing methods can be considered applicable to FMC because both share a similar composition, being primarily composed of Fe oxyhydroxides and Mn oxides (Mizell and Hein 2018; Ochromowicz, Aasly, and Kowalczuk 2021).

TMC's process designed for PMN aims to produce battery-grade nickel and cobalt sulfate for the lithium-ion battery market as well as copper cathodes. The manganese silicate, a byproduct of pyrometallurgical processing, is intended for sale to the ferromanganese and silicomanganese industries (AMC 2021), where it serves as an important deoxidizers in steel production (Boulby, Canaguier, and Donald 2023). The process combines pyrometallurgical treatment, similar to nickel laterite processing, with hydrometallurgical sulfuric acid leaching, a common technique in the base metals industry (AMC 2021).

Several theoretical studies on commercial FMC mining emphasize the need for additional mineral processing steps to mitigate dilution (Callies and Johnson 1989; Goto et al. 2009; Morgan 2006; SPC 2016; Wenzel 1987). However, few experimental studies have investigated beneficiation methods such as froth flotation, gravity separation, or magnetic separation to remove the substrate before metallurgical treatment (Allen, Abercrombie, and Rice 1991; Hirt, Rice, and Shirts 1991; Ito et al. 2008; Okamoto et al. 2018; Takahashi et al. 2023). For instance, Okamoto et al. (2018) reported a 96% FMC recovery using gravity separation with a jig.

Based on this information, the metallurgical processing route assumed in this study (Figure A1) includes a beneficiation step using gravity separation (jig), followed by a combined hydro-pyrometallurgical process designed to produce cobalt and nickel sulfate, copper cathodes, and manganese silicate.

3. Methodology

3.1. Data preprocessing and topographic delimitation

Raw bathymetric data were reprojected to WGS 84/UTM zone 55 N, resampled to a 10 m pixel size, and gaps filled *via* interpolation. Bathymetric data were restricted to depths of 800–2500 m and slopes $> 4°$, consistent with parameters believed to control FMC growth (Section 2.1). Within a 20 km^2 mining block, the restricted bathymetry was assumed to represent a stable, sediment-free surface of the FMC mineralization, forming the basis for the geological model. It was assumed that FMC form

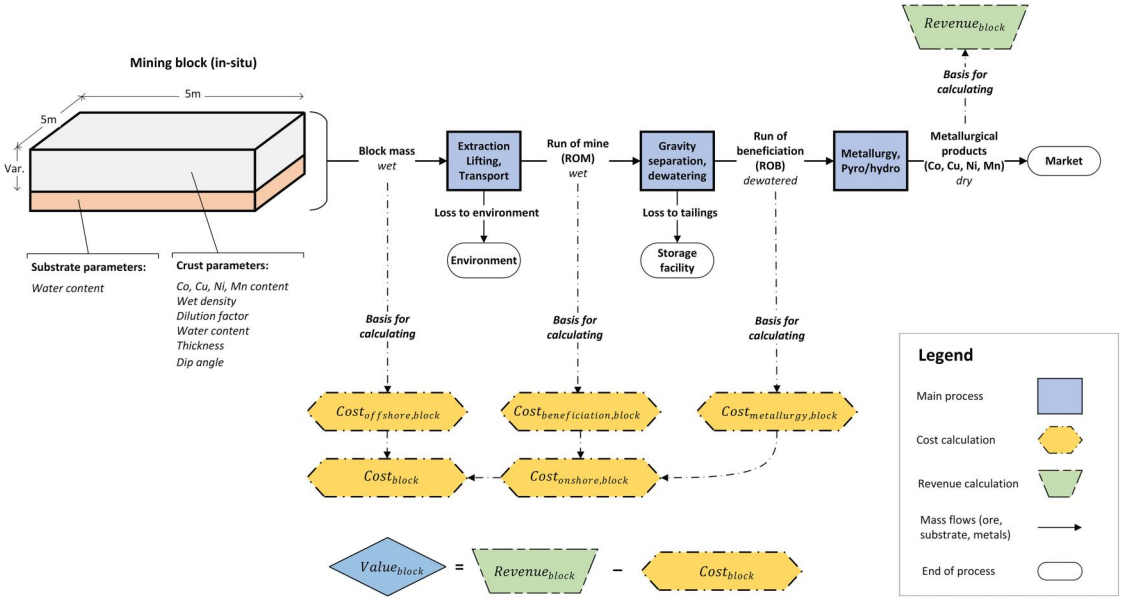

Figure 3. Schematic representation of the ore flow from in-situ ore blocks to the market, detailing material streams critical for revenue generation and cost analysis. The final block value is calculated from the block revenues and cost.

on stable substrates unaffected by mass-wasting events, enabling uninterrupted growth and the formation of a thick, continuous, pavement-like FMC layer.

3.2. Geological and economic block modeling

A synthetic, regularly spaced grid of drill holes was established across the hypothetical mine site. Each hole was defined by collar coordinates, dip (calculated from the local slope assuming perpendicular drilling), a fixed azimuth of 270°, arbitrary length, and lithological drill core intervals. Each drill hole was assumed to intersect two distinct layers—FMC overlying substrate—resulting in one drill core interval for each. The influence of slope angle on drill hole spacing was not considered. To populate the core intervals, FMC thicknesses were randomly sampled from an empirical cumulative distribution function (ECDF). Metal contents and wet bulk densities were sampled in the same manner. All sampled values were constrained by observed minimum and maximum values. To account for geological uncertainty, 50 sets of drill holes were simulated to generate 50 block models.

Using the delimited bathymetry and modeled FMC thicknesses, a volumetric model was built, which was then divided into equal 5 m × 5 m blocks with variables thicknesses. Radial basis function (RBF) interpolation (Hardy 1971; Powell 1992) was used to interpolate FMC thickness, metal content, and wet density values from the drill core intervals across the blocks. Dry bulk densities for each block were calculated from the interpolated wet densities and a fixed water content *via* Equation 4. Each block was also assigned a dip angle derived from the site's bathymetry and a fixed substrate water content.

An economic algorithm (Section 3.3) was applied to the geological block models to generate 50 EBMs. Blocks exceeding specific slope limits or falling below the required thickness were excluded as non-mineable. For each remaining block, the algorithm calculated its economic value based on extraction costs and revenues, retaining only those with a positive economic value. Selected input parameters were informed by SMS mining, reflecting anticipated similarities in seafloor topography (e.g., steep slopes), metocean conditions, water depth, and mining system configuration between prospective FMC and SMS extraction sites. Where necessary, price and cost figures were adjusted to 2023 dollars. The resulting EBMs served as the basis for sensitivity analyses.

3.3. Determining block economic value

Prior studies (Ellefmo 2022; Lesage, Juliani, and Ellefmo 2018) assign each block in the geological block model a monetary value ($\text{Value}_{\text{block}}$) equal to its revenue ($\text{Revenue}_{\text{block}}$) minus its cost ($\text{Cost}_{\text{block}}$), thereby deriving the EBM (Equation 1). Figure 3 illustrates the method developed and applied in this article that calculates block revenue and cost based on the flow of ore.

$$\text{Value}_{\text{block}} = \text{Revenue}_{\text{block}} - \text{Cost}_{\text{block}} \quad (1)$$

3.3.1. Revenue calculation

The selected metallurgical process model (Figure A1) recovers target metals from each ore block into several sellable products (n_{products}). The sum of revenues from each product ($\text{Revenue}_{\text{product}}$) equals the block revenue:

$$\text{Revenue}_{\text{block}} = \sum_{i=1}^{n_{\text{products}}} \text{Revenue}_{\text{product},\,i} \quad (2)$$

Similar to Lesage, Juliani, and Ellefmo (2018) and Volkmann (2019), the EBM computes each product's revenue from its selling price ($\text{price}_{\text{product},\,i}$), the dry mass of crust ($\text{mass}_{\text{dry, crust, block}}$), and losses during mining ($\eta_{\text{mining, block}}$), beneficiation ($\eta_{\text{beneficiation, crust}}$), and metallurgy

($\eta_{\text{metallurgy},i}$). All remaining metals are assumed to be converted into sellable products, represented by the ratio of the average dry metal grade (g_i) in the block to the grade in the final product ($g_{\text{product},i}$):

$$\text{Revenue}_{\text{product},i} = \text{mass}_{\text{dry,crust,block}} * \eta_{\text{mining,block}} * \eta_{\text{beneficiation,crust}} * \frac{g_i}{g_{\text{product},i}} * \eta_{metallurgy,i} * price_{product,i} \quad (3)$$

$\text{mass}_{\text{dry, crust, block}}$ is derived from the block volume ($\text{volume}_{\text{crust, block}}$) and dry bulk density ($\rho_{\text{crust, dry, block}}$). $\text{volume}_{\text{crust, block}}$ equals the product of the fixed block width (x_{block}) and length (y_{block}) as well as variable FMC thickness (z_{block}). $\rho_{\text{crust, dry, block}}$ is calculated from the FMC wet bulk density ($\rho_{\text{crust, wet, block}}$) adjusted by a fixed water content ($\text{water}_{\text{crust}}$):

$$\begin{aligned}\text{mass}_{\text{dry, crust, block}} &= \text{volume}_{\text{crust, block}} * \rho_{\text{crust, dry, block}} \\ &= x_{\text{block}} * y_{\text{block}} * z_{\text{block}} * \rho_{\text{crust, wet, block}} * (1 - \text{water}_{\text{crust}})\end{aligned} \quad (4)$$

The overall mining efficiency ($\eta_{\text{mining, block}}$) is the product of excavation ($\eta_{\text{excavation}}$), collection ($\eta_{\text{collection}}$), and transport ($\eta_{\text{transport}}$) efficiencies, assuming that each stage operates independently:

$$\eta_{\text{mining, block}} = \eta_{\text{excavation}} * \eta_{\text{collection}} * \eta_{\text{transport}} \quad (5)$$

3.3.2. Cost calculation

PMN operations divide operational expenditure (OPEX) into offshore mining costs ($\text{Cost}_{\text{offshore, block}}$) and costs for extractive metallurgy onshore ($\text{Cost}_{\text{onshore, block}}$) (Van Nijen, Van Passel, and Squires 2018). This same split is applied here to DSM operations for FMC:

$$\text{Cost}_{\text{block}} = \text{Cost}_{\text{offshore, block}} + \text{Cost}_{\text{onshore, block}} \quad (6)$$

Similar to onshore mining (Rudenno 2012), $\text{Cost}_{\text{offshore, block}}$ comprise the costs for ore extraction and transport (vertical lifting and horizontal transport) to the quayside. Lacking a commercially viable CMS, it is assumed that the mining company pays a rental cost (asset $\text{cost}_{\text{time}}$) for the marine assets, similar to time charter contracts (Karakitsos and Varnavides 2014). Thus, $\text{Cost}_{\text{offshore, block}}$ is calculated as the product of asset $\text{cost}_{\text{time}}$ and the time to mine an FMC block ($\text{time}_{\text{mining, block}}$):

$$\text{Cost}_{\text{offshore, block}} = \text{asset cost}_{\text{time}} * \text{time}_{\text{mining, block}} \quad (7)$$

Mining time equals the ratio of the total mined wet mass ($\text{mass}_{\text{mined, wet, block}}$) to the mining rate ($\text{mining rate}_{\text{period}}$):

$$\text{time}_{\text{mining, block}} = \frac{\text{mass}_{\text{mined, wet, block}}}{\text{mining rate}_{\text{period}}} \quad (8)$$

$\text{mass}_{\text{mined, wet, block}}$ is calculated by adjusting the wet mass of FMC ($\text{mass}_{\text{crust, wet, block}}$) with the dilution factor[1] ($\text{dilution}_{\text{wet, block}}$):

$$\begin{aligned}\text{mass}_{\text{mined, wet, block}} &= \frac{\text{mass}_{\text{crust, wet, block}}}{1 - \text{dilution}_{\text{wet, block}}} \\ &= \frac{\text{volume}_{\text{crust, block}} * \rho_{\text{crust, wet, block}}}{1 - \text{dilution}_{\text{wet, block}}}\end{aligned} \quad (9)$$

The mining rate is calculated by multiplying the nominal mining rate ($\text{mining rate}_{\text{nominal, period}}$) by an availability factor ($\alpha_{\text{offshore system, period}}$) that accounts for system downtime, similar to Lesage, Juliani, and Ellefmo (2018):

$$\text{mining rate}_{\text{period}} = \text{mining rate}_{\text{nominal, period}} * \alpha_{\text{offshore system, period}} \quad (10)$$

$$0 \leq \alpha_{\text{offshore system, period}} \leq 1 \quad (11)$$

$\text{Cost}_{\text{onshore, block}}$ splits into a beneficiation cost ($\text{Cost}_{\text{beneficiation, block}}$) and metallurgical processing cost ($\text{Cost}_{\text{metallurgy, block}}$):

$$\text{Cost}_{\text{onshore, block}} = \text{Cost}_{\text{beneficiation, block}} + \text{Cost}_{\text{metallurgy, block}} \quad (12)$$

A block's beneficiation cost is computed by multiplying the cost per ton ($\text{Cost}_{\text{beneficiation, ton}}$) by the run-of-mine[2] wet mass ($\text{ROM}_{\text{wet, block}}$):

$$\text{Cost}_{\text{beneficiation, block}} = \text{Cost}_{\text{beneficiation, ton}} * \text{ROM}_{\text{wet, block}} \quad (13)$$

$\text{ROM}_{\text{wet, block}}$ is obtained as the product of the mined wet mass and the mining efficiency:

$$\text{ROM}_{\text{wet, block}} = \text{mass}_{\text{mined, wet, block}} * \eta_{\text{mining, block}} \quad (14)$$

For metallurgical processing, a dewatered run-of-beneficiation[3] ($\text{ROB}_{\text{dewatered, block}}$) is introduced, which represents the dewatered concentrate sent to metallurgical processing. Consequently, $\text{Cost}_{\text{metallurgy, block}}$ is calculated as the product of the cost per ton ($\text{Cost}_{\text{metallurgy, ton}}$) and $\text{ROB}_{\text{dewatered, block}}$:

$$\text{Cost}_{\text{metallurgy, block}} = \text{Cost}_{\text{metallurgy, ton}} * \text{ROB}_{\text{dewatered, block}} \quad (15)$$

$\text{ROB}_{\text{dewatered, block}}$ is the sum of the recovered FMC mass ($\text{mass}_{\text{crust, beneficiation}}$) and substrate mass ($\text{mass}_{\text{substrate, beneficiation}}$):

$$\text{ROB}_{\text{dewatered, block}} = \text{mass}_{\text{crust, beneficiation}} + \text{mass}_{\text{substrate, beneficiation}} \quad (16)$$

The mass of FMC and substrate are calculated based on their proportions in $\text{ROM}_{\text{wet, block}}$ and their respective beneficiation recoveries ($\eta_{\text{beneficiation, crust}}$ and $\eta_{\text{beneficiation, substrate}}$), while correcting for water content ($\text{water}_{\text{crust}}$ and $\text{water}_{\text{substrate}}$):

$$\text{mass}_{\text{crust, beneficiation}} = \text{ROM}_{\text{wet, block}} * (1 - \text{dilution}_{\text{wet, block}}) * \eta_{\text{beneficiation, crust}} * (1 - \text{water}_{\text{crust}}) \quad (17)$$

$$\text{mass}_{\text{substrate, beneficiation}} = \text{ROM}_{\text{wet, block}} * \text{dilution}_{\text{wet, block}} * \eta_{\text{beneficiation, substrate}} * (1 - \text{water}_{\text{substrate}}) \quad (18)$$

3.4. Sensitivity analysis

The sensitivity analysis, conducted across 50 EBMs, varied selected input parameters by ±20% to create high- and low-case deposit value scenarios (Equation 19). Boxplots highlighted the primary drivers of deposit value generation, helping to inform CMS design requirements. A parameter was considered sensitive if its interquartile range (25th–75th percentile) lay entirely above or below zero. The analysis included cumulative metric curves and marginal metric curves for selected sensitive engineering parameters (e.g., deposit value vs parameter setting) to illustrate parameter influence on EBM results. Marginal curves were derived by computing the discrete change in cumulative metrics between successive parameter increments (i.e., stepwise differences), and their derivatives were analyzed to identify inflection points. Figure A2 illustrates a schematic representation of the methodology employed in this study.

$$\text{Deviation from base case}_i = \text{Deposit value}_{\text{Scenario},\,i} - \text{Deposit value}_{\text{base case},\,i} \quad (19)$$

4. Materials and data

Bathymetry data (147°–149°E, 20°–21°N) sourced from NOAA (2023) (pixel size approximately 100 m), along with FMC thickness (Table A1) and metal content data (Table A2), were the primary inputs for creating the geological block model. The base case input parameters for developing the EBMs include FMC physical properties (Table A3), metallurgical processing parameters (Table A4), and metallurgical products, along with their metal contents and estimated market prices (Table A5), with details of the price calculations provided in Table A6. Additional required inputs included the system's overall mining efficiency (Table A7), annual mining rate (Table A8), and operating costs (Table A9). Onshore processing costs for both beneficiation and extractive metallurgy are presented in Table A10. A dilution factor of 25% was applied, based on estimates by Halkyard (1985) and Morgan (2006). To account for performance reduction due to system downtime, an overall marine assets availability was introduced, following Lesage (2019). Given the absence of an existing CMS, this study assumes an annual system availability of 84%, as proposed by SRK Consulting (2010) for SMS mining. The interpolation parameters for the RBF method are listed in Table A11.

Limited literature exists on FMC mining machine slope operation. While tracked machines generally require gentle slopes, Remotely Operated Vehicle (ROV)-type or thruster-assisted machines may operate on slopes up to 25° (I. Maskell, Assessing the Operating Slope Angle for a Co-Rich Crust Mining Machine, pers. comm., July 17, 2024). Thus, the base case scenario assumes an operating slope angle of 25°. A cut-off FMC thickness of 40 mm, as suggested by Hein et al. (1998, Hein, Conrad, and Dunham 2009), was applied in this study.

A sensitivity analysis examined 13 EBM input parameters related to CMS performance and economics. Table 2 presents all base case input parameters alongside their respective high and low case values.

4.1. Software

QGIS version 3.34.5 (QGIS.org 2024) was used for the preprocessing and manipulation of bathymetric data, initial delimitation of the prospective FMC extraction area, and implementation of the simulated drill holes. The geological model and resulting block models were created using Leapfrog Geo version 2023.2.1 (Seequent, n.d.). Python version 3.11.7 in Spyder 5.5.1, in combination with libraries pandas (McKinney 2010; The Pandas Development Team 2020), NumPy (Harris et al. 2020), Matplotlib (Hunter 2007), and Seaborn (Waskom 2021), was implemented to simulate the metal grades, FMC thicknesses, and wet densities across the drill holes, calculate the EBMs, perform the sensitivity analyses, and create the respective figures. The spreadsheets containing drill hole data (collar table, survey table, interval table) imported to Leapfrog Geo were created in Microsoft Excel version 2402. ChatGPT-4, Microsoft Copilot, and Grammarly were utilized to enhance the readability of the manuscript. ChatGPT-4 was used to identify and correct errors in the Python scripts.

Table 2. Selected input parameters for the sensitivity study. All values are rounded to the nearest whole number.

Parameter	Unit	Base case values	Low case value (−20%)	High case value (+20%)
System availability	%	84	67	100
Dilution (wet)	%	25	20	30
Mining efficiency	%	75	60	90
Price Cu cathodes	USD/t	8237	6590	9885
Price Ni sulfate	USD/t	4687	3749	5624
Price Co sulfate	USD/t	8385	6708	10,062
Price manganese silicate	USD/t	230	184	276
Nominal mining rate	Million tons per annum	1	0.8	1.2
Cost asset time	USD/day	165,770	132,616	198,924
Cost beneficiation	USD/wet ton	8	7	10
Cost metallurgy	USD/dry ton	136	109	163
Mineable slope angle	°	25	20	30
Mineable crust thickness	mm	40	32	48

Table 3. Summary statistics of simulated metal grades for the first 10/50 block models (all values in %).

Block model	1	2	3	4	5	6	7	8	9	10
Mean Co	0.42	0.43	0.43	0.39	0.42	0.43	0.40	0.42	0.40	0.38
Median Co	0.41	0.41	0.41	0.37	0.39	0.42	0.38	0.39	0.38	0.36
Standard deviation Co	0.18	0.19	0.18	0.16	0.19	0.17	0.19	0.16	0.16	0.17
CV Co	43.25	44.46	41.36	41.41	45.04	38.54	47.20	37.55	39.84	44.52
Mean Ni	0.27	0.27	0.29	0.26	0.28	0.27	0.28	0.27	0.29	0.26
Median Ni	0.26	0.26	0.27	0.25	0.27	0.25	0.27	0.27	0.28	0.26
Standard deviation Ni	0.11	0.11	0.10	0.10	0.11	0.11	0.12	0.10	0.11	0.10
CV Ni	41.39	40.79	34.91	39.72	40.52	40.25	42.60	37.59	36.93	37.88
Mean Cu	0.06	0.06	0.06	0.06	0.05	0.05	0.06	0.06	0.06	0.06
Median Cu	0.05	0.05	0.05	0.05	0.05	0.05	0.05	0.06	0.05	0.05
Standard deviation Cu	0.03	0.03	0.03	0.03	0.03	0.03	0.03	0.03	0.03	0.03
CV Cu	51.43	49.31	53.42	51.32	54.00	55.01	48.90	43.49	53.44	49.49
Mean Mn	20.33	20.80	21.11	20.89	20.69	21.42	21.12	20.50	21.90	20.26
Median Mn	20.37	20.50	21.00	20.68	20.77	21.22	21.12	20.68	21.89	20.39
Standard deviation Mn	4.67	4.97	4.60	4.60	4.46	4.44	4.48	4.65	4.54	4.90
CV Mn	22.96	23.89	21.80	22.02	21.56	20.72	21.22	22.70	20.72	24.19

CV, coefficient of variation. Mean values are non-weighted.

Table 4. Unweighted average EBM parameters for the base case scenario, calculated across 50 EBMs (each representing a single 15 km^2 hypothetical mine site).

Parameter	Average value	Standard deviation	Unit
In-situ wet mass	353,238	83,477	t
Run of mine (ROM)	470,984	83,477	t
Number of positive-value blocks	71,110	16,913	–
Wet mass per block	6.64	0.47	t
Areal abundance	199	14	Wet kg/m^2
Life of mine (LOM)	205	48	days

Ore blocks are constrained to positive USD values. All figures are rounded to whole numbers unless otherwise displayed. Note that number of ore blocks varies between EBMs, resulting in non-integer average values.

Table 5. Average cost for the base case scenario, calculated across 50 block models and expressed per mined wet tons of ore (ROM).

Parameter	USD/wet t mined	Percentage (%)
Mining cost	96	57
Beneficiation cost	8	5
Metallurgy cost	65	38
Total cost	169	100

Blocks are constrained to positive USD values. All figures are rounded to two decimal places.

5. Results and discussion

5.1. Ferromanganese crust growth zone

A ring-shaped FMC growth zone (CGZ) was delineated between approximately 1500 and 2500 m depth, covering about 492 km^2 with slope angles ranging from 4° to 72° (blue/white area in Figure 4A). Its shape is consistent with FMC deposits observed in the Pacific (Du et al. 2018, 2020; Novikov et al. 2014). From the CGZ, a hypothetical 15 km^2 mine site was identified (Figure 4B), with slope angles ranging from 4° to 43° and nearly 100% hypothetical FMC coverage. Both the CGZ and hypothetical mine site align with Josso and Hall's (2022) prospectivity map (Figure A3), although the map also indicates likely FMC occurrence on the summit—consistent with recent observations of FMC outcrops on guyots (Hino et al. 2024; Hino and Usui 2022; Yeo et al. 2019). The guyot's predominantly flat summit was excluded from the assessment due to an assumed thick sediment layer that could hinder mining operations. However, since FMC deposits may occur beneath summit seamount sediments (Neettiyath et al. 2022; Yamazaki and Sharma 1998), future research should assess the resource potential of both slopes and summits and consider implications for CMS design. Extracting FMC buried under sediment layers will require an additional function for sediment removal prior to extraction.

5.2. Spatial variability of block model parameters

Table 3 summarizes statistics for ten simulated block models in the base case scenario. Compared to the values reported in the literature (e.g., Hein et al. (2013) for samples in the PCZ) the mean metal grades observed here are lower. An exemplary model shows clusters of high and low metal grades, FMC thickness and wet density (Figure 5). The 647,117 blocks displayed reveal gaps where slopes are below 4°, indicating no FMC. The spatial heterogeneity in metal grades reflects the coefficient of variation from the interpolation process (Table 3). This patchy distribution results from the interpolation method applied to a regular drill grid. However, there is no conclusive evidence that this pattern reflects the true parameter variability of an FMC deposit. Previous studies have shown correlations between FMC composition and depth (Hodkinson and Cronan 1991; Usui et al. 2017), indicating that future EBMs could improve accuracy by integrating these relationships.

5.3. EBM

Following the methodology presented in Section 3, only ore blocks with a positive USD value are considered mineable. The average economic value per wet ton of ore is 17 USD, with EBM total values ranging from 2.76 to 10.02 MUSD and a median of 5.97 MUSD (Figure 6). Figure 7B shows an exemplary EBM with sparse distribution of positive-value ore blocks across the mine site, indicating that mining and metallurgy costs assumed in this case largely offset revenues from metal sales. Table 4 summarizes parameters for positive-value blocks across 50 base case EBMs. On average, 71,110 ore blocks—approximately 11% of all blocks within the EBM—yield positive values, equivalent to 470,984 wet tons mined over the life of mine (LOM). The LOM ranges

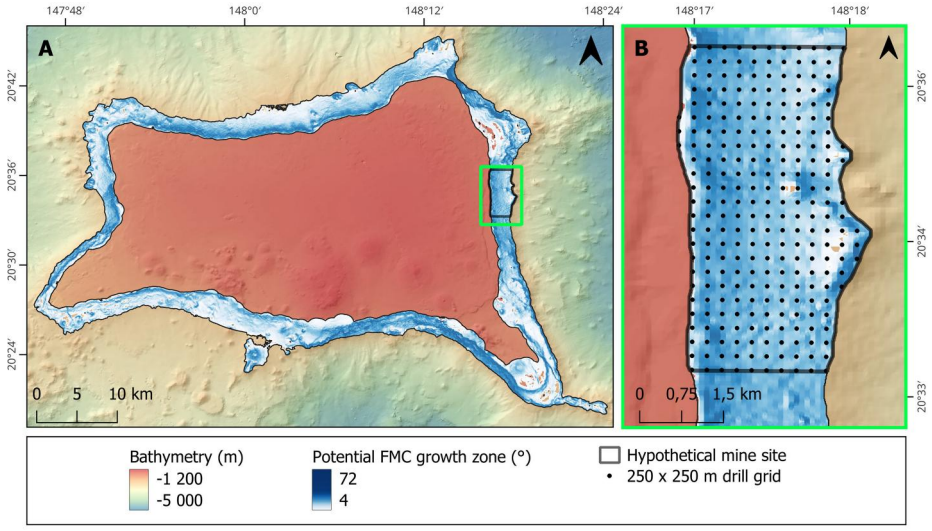

Figure 4. Ring-shaped zone of potential FMC growth limited to the edges of Fryer guyot's summit and its upper slopes. The topographical segment on the Eastern flank was used as input for the geological deposit model (A). Selected hypothetical mine site with hypothetical drill grid of 250 m by 250 m containing a total of 256 drill holes (B). Bathymetric data from NOAA (2023).

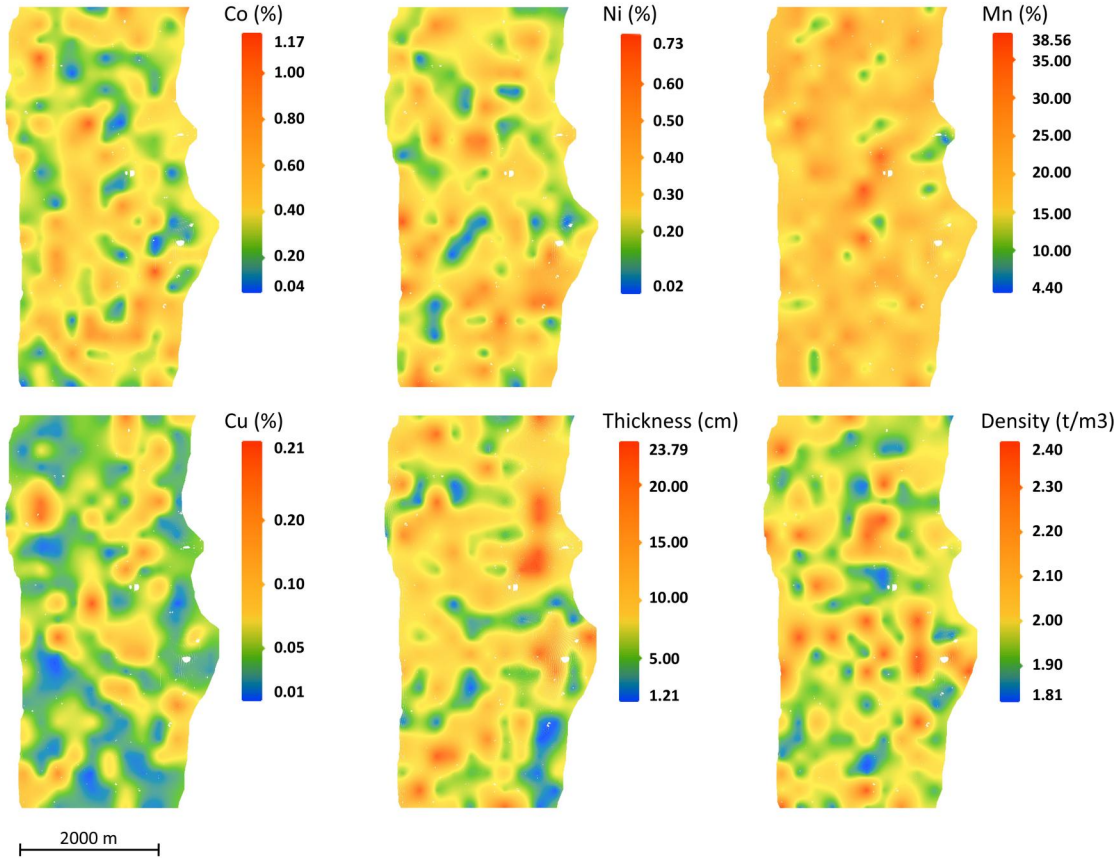

Figure 5. Top-down view of block model 30 showing interpolated grades for Co (0.04–1.17%), Ni (0.02–0.73%), Mn (4.4–38.56%), and Cu (0.01–0.21%) as well as FMC thickness (1.21–23.79 cm) and wet density (1.81–2.4 t/m^3) across the hypothetical mine site. Distributions are derived from interpolation of simulated drill hole data.

between 110 and 352 days, averaging 205 days. If the full 492 km^2 CGZ were mined by partitioning it into 15 km^2 blocks—each with an average LOM of 205 days—Fryer Guyot could accommodate roughly 33 mine sites, resulting in an overall LOM of about 18.2 years. The average areal abundance of wet FMC aligns with literature values (Hino and Usui 2022). Using an approximate 32% water content for FMC (Table A3) yields results consistent with recent

areal abundance estimates for a single Pacific guyot (averaging 145 dry kg/m^2; Hwang et al. (2024)), suggesting the model reasonably reflects actual FMC deposit conditions.

Figure 8 illustrates that revenue is primarily driven by cobalt sulfate (50%) and manganese silicate (32%), positioning an FMC mining operation as mainly a cobalt-manganese venture—unlike a PMN mining operation, which is essentially a nickel-manganese venture (AMC 2021). However, the future market for cobalt sulfate remains uncertain amid evolving battery chemistries and cobalt-efficient alternatives (IEA 2024b). Similarly, although PMN-derived manganese silicate is viable for silicomanganese production (Boulby, Canaguier, and Donald 2023), the market potential for manganese silicate from FMC remains speculative. Nickel sulfate contributes 16% to revenue, while copper, at 1%, plays a minimal role due to the low average grades (Table A2), which are about half the NW Pacific average (Hein et al. 2017), though actual FMC mining could yield higher contributions. The average revenue per wet ton mined is 186 USD, with total deposit revenues ranging from 34.79 to 112.52 MUSD and a median of 64.57 MUSD (Figure 6).

Production costs amount to 169 USD per ton of wet ore, distributed as 57% mining, 38% metallurgical processing, and 5% beneficiation (Table 5). The significant share attributed to mining costs underscores the importance of minimizing these costs in CMS design. Total production costs (offshore and onshore cost) range from 32.03 to 102.85 MUSD, with a median of 57.9 MUSD (Figure 6). High mining and metallurgical processing costs (Table 2), coupled with a cobalt recovery rate of only 77.2% (Table A4), contribute to lower deposit values.

5.4. Processing route

Given the low cobalt recovery rate (Table A4), future FMC processing designs should focus on improving cobalt extraction. Alternative processing routes, such as the process by Mittal and Sen (2003) for PMN, could achieve similarly high cobalt recoveries (80%) when applied to FMC. Additionally, Malnic (2008) reported superior recoveries of Ni, Co, Cu, and Mn from FMC using a nickel-laterite process, while Jiang et al. (2016) observed high extraction rates for Ni, Co, and Cu during continuous leaching tests on FMC-PMN mixtures. While these alternatives could improve FMC economics, the current TMC route yields a more conservative EBM that can be refined as additional processing data become available. In addition, although rare metals were excluded from current economic calculations, extracting rare earth elements (REEs) and/or tellurium (Hein, Koschinsky, and Halliday 2003), could improve FMC mining profitability (Goto et al. 2009) if suitable processing methods are developed and feasibility studies completed. Researchers should further investigate PMN-focused processing routes for FMC, as well as the potential benefits of blending both mineral types, as demonstrated by Jiang et al. (2016).

5.5. Sensitivity analysis

Key parameters affecting CMS engineering design were evaluated (Figure 9). The five most sensitive parameters include mining efficiency, daily charter rate, cobalt sulfate price, mining rate, and system availability. Mining efficiency exerts the greatest influence, outweighing external factors like cobalt sulfate and manganese silicate prices, which are beyond the designer's control. Therefore, mining efficiency should be prioritized during the design of the CMS. Improving mining efficiency by 20% increases deposit value by a median of 11.1 million USD. As illustrated in Figure 7C, this enhancement results in larger and more interconnected ore patches. Similarly, a 20% reduction in the daily charter rate contributes a median gain of 10.8 million USD. Increases in the nominal mining rate and system availability add median values of 8.4 and 7.9 million USD, respectively. In contrast, ore dilution and mineable slope angle show lower sensitivity—though the mineable slope angle is more sensitive in the low case, as 72% of the blocks fall below the

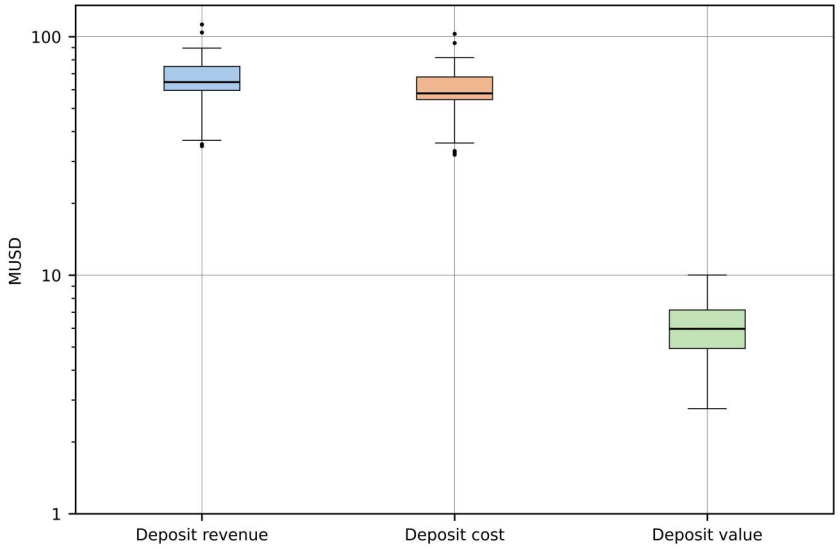

Figure 6. Distribution of deposit revenue, cost, and value across 50 base case block models, considering only ore blocks with a positive value.

base case value of 25°. Commodity prices of cobalt sulfate and manganese silicate are highly influential, while nickel sulfate and copper cathode prices have less impact due to their relatively lower ore grades. Other parameters, including beneficiation cost and mineable crust thickness deviate little from the base case, indicating lower sensitivity. The deposit value is insensitive to variations in the mineable crust thickness, since the majority of ore blocks exceed the high-case value of 48 mm (Table 2).

5.5.1. Mineable slope angle

Although less sensitive than other parameters (Figure 9), the mineable slope angle plays a critical role in FMC mining machine design. The available FMC tonnage—and thus the deposit value—levels off around a 32° slope because fewer positive-value blocks are available on steeper slopes (Figure 10A and C). Marginal gains (Figure 11A) accelerate up to the 12.5–15° inflection point, and then peak at approximately 1.7 million USD when the mineable slope angle increases from 20° to 22.5°. Therefore, a CMS should be designed for at least 15° to capture accelerating marginal gain, and optimally to 22.5° to maximize those gains. Slopes above 32° yield little additional value and can be deprioritized.

Previous research on a Pacific seamount focused on slopes <10° due to anticipated mining system limitations (Hwang et al. 2024). However, prospectivity mapping suggests a high likelihood of FMC deposits on steeper slopes (Josso et al. 2023), and studies in the Norwegian Sea indicate that FMC form on slopes greater than 20° (Pedersen et al. 2021). Although pilot FMC mining machines have demonstrated limited success operating on slopes up to 29° (Orita et al. 2022; Xie, Chen, et al. 2022), further research is needed to develop design solutions that can ensure reliable operation on steep seamount flanks.

5.5.2. Mineable crust thickness

Most ore blocks in the EBMs exceed 5 cm in thickness. As a result, cumulative ore tonnage and deposit value are maximized when the mineable FMC thickness is just below 5 cm (Figure 10B and D). However, if the FMC mining machine was, for example, restricted to extracting only FMC thicker than 10 cm, the deposit's value would decrease by approximately 2.5 million USD (Figure 10D). Marginal value loss increases, reaching its maximum at a mineable crust thickness of 10 cm (see trough in Figure 11B), then declines as fewer blocks remain available for extraction. To minimize value losses, the mineable FMC thickness should stay below 10 cm—ideally below 5 cm—as marginal losses accelerate approaching the 3.75–5 cm inflection point.

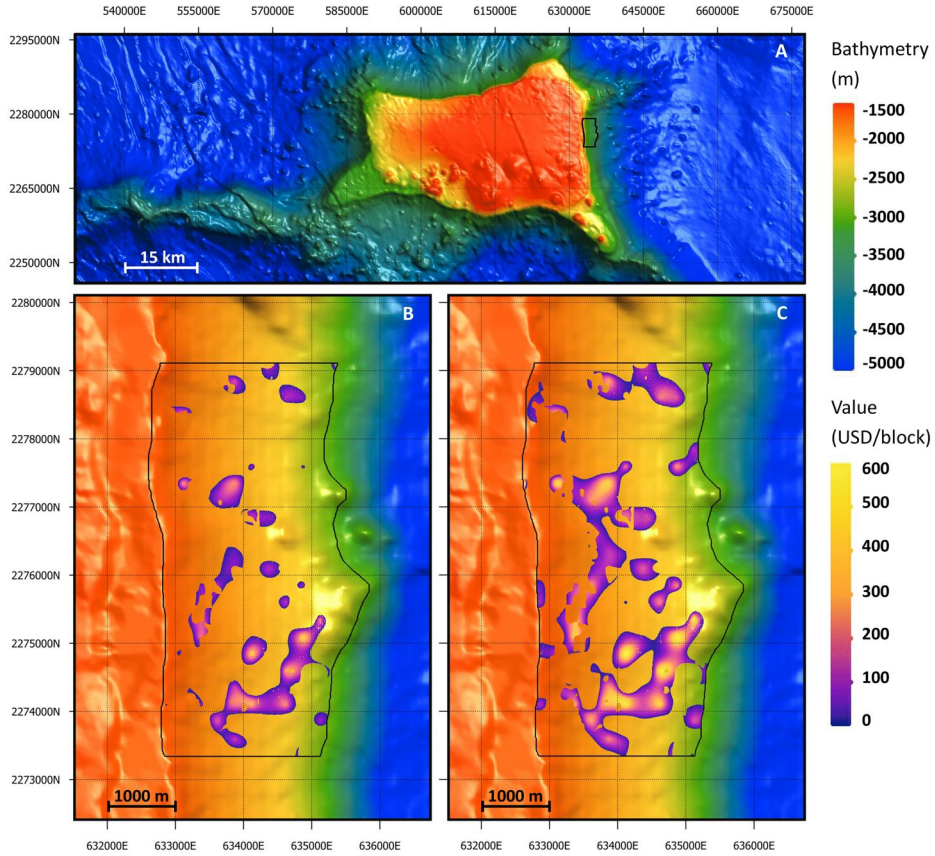

Figure 7. Plan view of Fryer Guyot (A) illustrating the mineable portion of block model 30 under the base case scenario (B) and with a 20% increase in mining efficiency (C). Areas colored from purple to yellow represent blocks with a positive value, located on slopes between 4° and 25°, with FMC thicknesses greater than 4 cm. The total number of blocks with a positive value is 77,532 in the base case (B) and 156,371 with increased mining efficiency (C). Blocks are displayed over a 10-m resolution bathymetric map of the seamount flank, with the black line indicating the boundary of the hypothetical mine site (compare Figure 4). Bathymetric data from NOAA (2023).

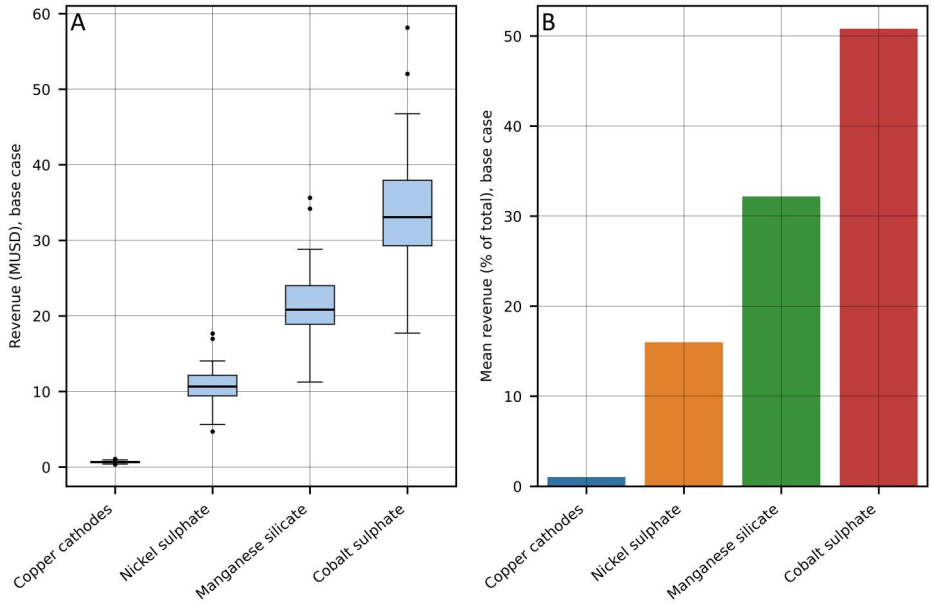

Figure 8. Revenue distribution by metallurgical product (A) and average revenue contribution per metallurgical product across all block models (B) in the base case scenario.

5.5.3. Mining efficiency

A mining efficiency below 40% yields no positive-value blocks (Figure 12A), marking this as the minimum viable threshold. From such low efficiency, only high-grade blocks generate enough revenue to offset extraction costs. The inflection point suggests that a mining efficiency of at least 80% is desirable to capture accelerating marginal deposit values. Beyond 80%, marginal gains remain relatively constant. In the base case, overall mining efficiency (75%) accounts for 25% of metal losses, indicating significant room for improvement. This metric is calculated based on a 90% excavation efficiency expected for SMS mining (Table A7), although FMC excavation efficiency estimates range between 30% and 82% (Goto et al. 2009; Hein 2006; Morgan 2006). A recent FMC pilot test achieved only 39% to 71% excavation efficiency, deemed insufficient for commercial viability (Orita et al. 2022). These variations emphasize the need for further research into FMC excavation methods. For example, Orita et al. (2022) detailed a horizontal drum cutter design, while Chinese researchers (Xie, Chen, et al. 2022; Xie, Wang, et al. 2022) explored different cutting modes. Loke Minerals envisions a mining machine with multiple rotary cutting heads to adapt for FMC micro-topography (Halvorsen 2022).

5.5.4. Mining rate

Figure 12B shows a minimum viable mining rate of 0.6 million tons per year. The inflection point suggests that a mining rate of at least 0.9 million tons per year is desirable, which aligns with literature (Goto et al. 2010). As the mining rate increases, offshore costs per block decrease, gradually making lower-revenue blocks available for extraction. Marginal deposit value peaks at 1.5 million tons per year, establishing this as a practical target for a CMS. However, more efficient processing methods, inclusion of additional metals, and evolving commodity markets could enable a higher mining rate, warranting further research.

5.5.5. System availability

System availability (Figure 12C) affects the mining rate (Equation 10). Reduced system availability increases offshore costs per block, while higher availability lowers them. A minimum of 45% availability is required for ore blocks to become available for extraction. A target of 75% is considered practical, capturing the benefits of accelerating marginal gains, as indicated by the 70–75% inflection point. TMC projects its PMN production system will operate 267 days per year (AMC 2021) (approximately 73% availability), which closely aligns with this practical target mentioned here.

5.5.6. Ore dilution

Increasing dilution from 0% to 5% results in the loss of approximately 32,000 ore blocks (Figure 12D), highlighting the importance of minimizing dilution. The maximum possible dilution is 60%, beyond which no mineable blocks remain. The 25–30% inflection point indicates that dilution should be maintained below 30% to avoid entering a zone of accelerated marginal value loss. Recent studies have mapped the distribution of seafloor types associated with FMC on various seamounts (Huang et al. 2024; Yeo et al. 2019). However, future research should investigate how substrate types beneath FMC in potential mining areas vary and how these variations might contribute to dilution during extraction. For example, differences in physical substrate properties (Hein et al. 2000) and variations in the adhesive bond between FMC and the underlying substrate could play a significant role (Halkyard 1985). Research shows that the physical properties of FMC, such as porosity and density, differ among layers (Hino and Usui 2022), which may also affect dilution. Several studies indicate that metal content, particularly cobalt, is higher in the upper FMC layers and declines closer to the substrate (Halbach and Manheim

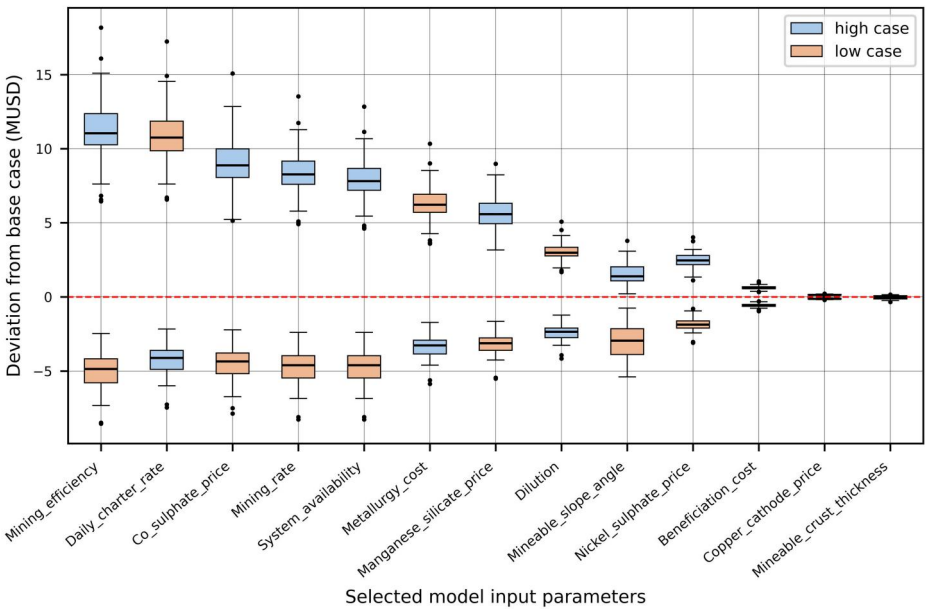

Figure 9. Boxplots showing the results of the sensitivity analysis, including the minimum and maximum values not considered outliers (whiskers), lower quartile (lower edge), median (centerline), and upper quartile (upper edge) for a set of 13 input parameters under both the low case and high case scenario. Outliers are indicated by a black dot. Each boxplot represents the distribution of deposit values across 50 block models, where a single input parameter is adjusted by either +20% or −20%. Both scenarios are depicted with separate boxplots, illustrating the range of deviations from the base case deposit value. The boxplots are ordered based on the difference in median values between the high and low case scenarios. The spread in the data, reflected by the length of the boxplot whiskers, is a result of the simulation of the deposit's geological conditions.

1984; Konstantinova et al. 2017; Wiltshire, Wen, and Yao 1999). This metal grade variation could have important implications for mining system design and warrants further investigation. A trade-off analysis is needed to determine whether extracting FMC in bulk down to the substrate or selectively mining the cobalt-rich upper layers would be more effective. The selective approach may help reduce dilution and improve economic returns.

5.5.7. Cost considerations

The CMS daily rate is crucial in determining deposit value, so incorporating it during the design phase is essential. Sensitivity analysis further reveals that reducing metallurgical costs through engineering improvements can significantly enhance value, highlighting metallurgical process design as an important lever. Figures 11 and 12 show that the average marginal deposit value is strongly influenced by

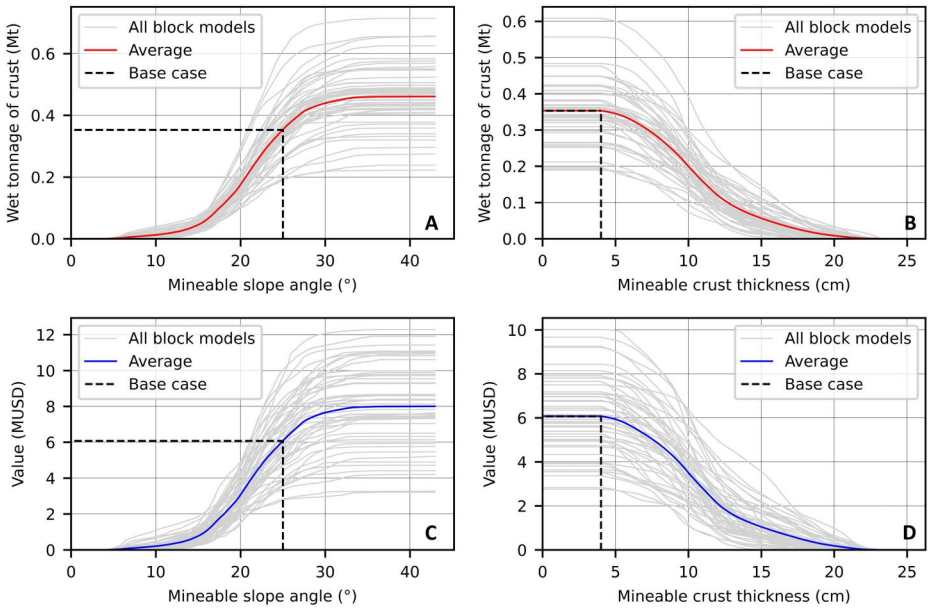

Figure 10. Influence of slope angle and FMC thickness on available FMC tonnage and deposit value in the base case scenario, considering only blocks with positive economic value. The red and blue curves indicate the average values across all 50 block models. The black dashed line represents the respective base case parameters.

key engineering parameters. Decision-makers must balance additional costs against the value that is unlocked through optimization. For example, designing a mining machine capable of mining steeper slopes could incur development, capital, and operational costs that outweigh the potential increase in marginal gain. Similarly, increasing the mining rate enhances overall deposit value, yet its economic feasibility depends on whether marginal gains justify associated costs. While the current framework aids decision-making, further research is needed for a comprehensive trade-off analysis based on detailed system design studies.

5.6. Challenges and adaptations for FMC mining on seamounts

Figure 7 suggests several potential challenges for FMC mining machines. With FMC patches more than 1000 m apart, the machines must operate on inclined, sediment-free seamount flanks to selectively extract high-value ore zones—likely requiring frequent relocation. Depending on the specific seamount and its distribution of slope angles, these machines may encounter a wide range of slopes (Figure 4), potentially necessitating custom design solutions tailored to the site's topography. Relocation could be achieved through self-propulsion, similar to existing DSM machines (AMC 2021; Peacock 2023), or *via* lifting wire transport (SRK Consulting 2010), each presenting trade-offs in mobility, speed, cost, and complexity that require further study. To minimize production disruptions, potential strategies include stockpiling ore as a buffer or deploying multiple FMC mining machines for continuous output. Initial extraction will likely prioritize the ore patches with the highest value to maximize early project cash flow and recover initial capital investments (Runge 1998). Thus, determining the optimal starting point, mining sequence, and mining direction are critical mining engineering challenges that require further study.

The above-mentioned challenges can be used to evaluate the latest DSM technology for its potential application to FMC mining. The mining system architectures of PMN operations in the CCZ (AMC 2021; Peacock 2023) share four core components—self-propelled seafloor mining tools, vertical lifting systems, support vessels, and transport barges. Given the similar metocean conditions in both the CCZ and PCZ (BPC, 2024; NORI, 2022), general system components like the vertical lifting system, support vessel, and transport barges, could potentially be adapted for FMC mining. However, differences in seafloor substrate are likely to pose a key challenge. Designed for the CCZ's soft and gently sloping (up to 6°) prospective mining areas (AMC 2021), TMC's PMN collector would likely face limitations on FMC-hosting seamounts. Its track area and submerged weight are influenced by the deep-sea clay's bearing capacity (AMC 2021), whereas firmer guyot substrates with steeper slopes (15.1° ± 4°) (Vogt and Smoot 1984) require redesigns in weight distribution and track system to prevent slippage, tipping, and pitch instability. Moreover, while PMN collectors follows a strip-mining approach requiring limited mobility, FMC mining must address patchy ore distributions (Figure 7) and micro-topographical challenges, likely needing enhanced pitch, yaw, and roll responsiveness. An FMC mining machine would also need an extra FMC extraction mechanism and

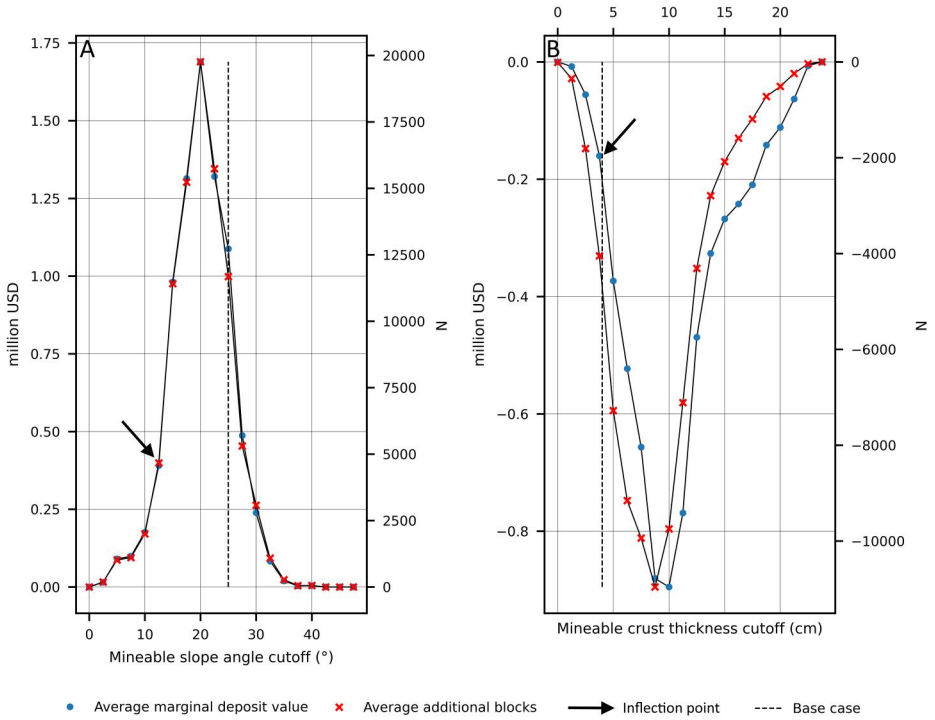

Figure 11. Marginal deposit value and marginal number of blocks as functions of mineable slope angle and mineable crust thickness. The tick labels indicate the lower bound of the parameter interval used to compute the marginal values; values are averaged across 50 block model realizations.

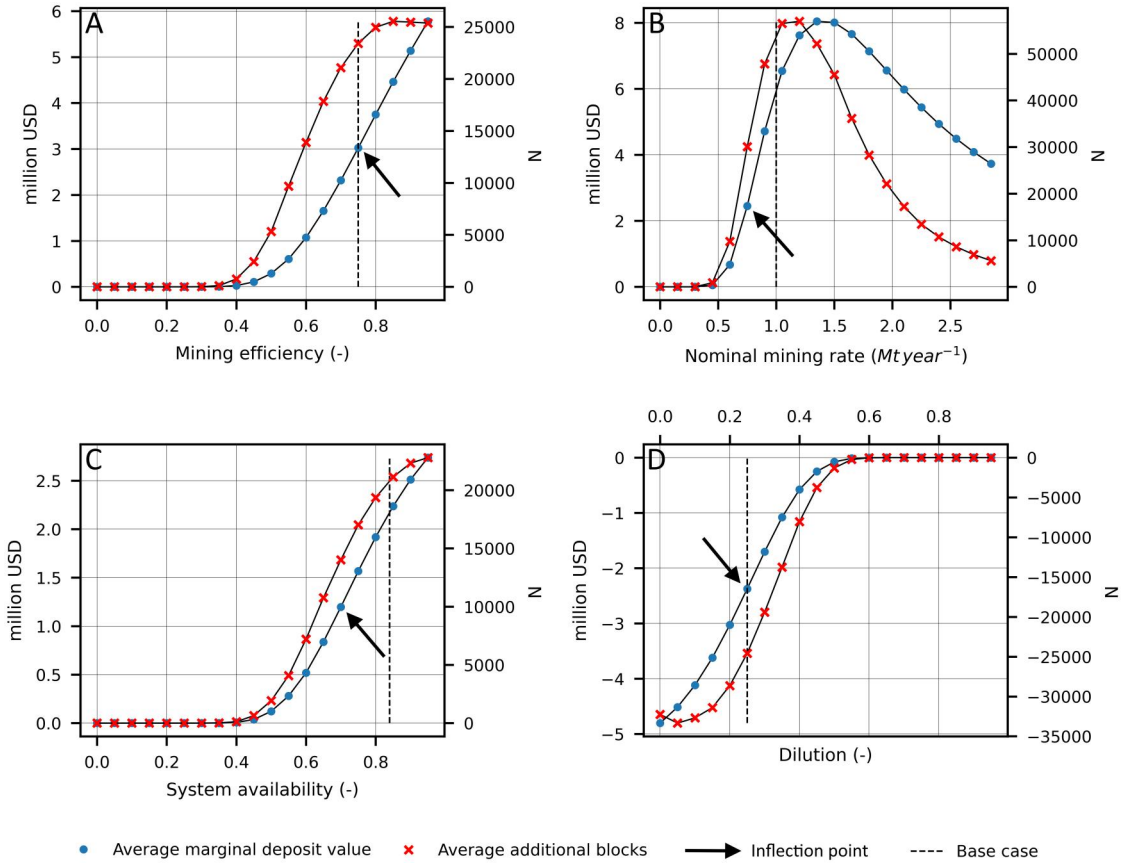

Figure 12. Marginal deposit value and marginal number of blocks in response to changes in input parameters. The tick labels indicate the lower bound of the parameter interval used to compute the marginal values; values are averaged across 50 block model realizations.

an improved collection mechanism to control gravitational down-slope movement of extracted ore. Although many PMN collector components (electric motors, hydraulic power units, buoyancy elements, telemetry systems, etc.) (AMC 2021; BGR, 2018) may be transferable, dedicated design studies are necessary to develop effective extraction, collection and propulsion solutions for seamount environments.

Table 6 summarizes the tentative design requirements for a CMS.

5.7. Limitations and uncertainties

Because direct evidence for an FMC deposit at Fryer Guyot is lacking, practical criteria such as water depth and slope angle were used to delineate its extent, introducing considerable uncertainty. Moreover, tectonic activity or mass-wasting events (Halbach and Manheim 1984; Hein et al. 2000; Hino et al. 2024; Novikov et al. 2014) may have fragmented FMC coverage beyond what the current model (Figure 4) reflects. These criteria likely oversimplify the deposit's complex morphology, potentially leading to an overestimation in spatial extent and volume. In addition, the impact of buried FMC layers (Neettiyath et al. 2022; Yamazaki and Sharma 1998) on total FMC volume cannot yet be accounted for.

The geological block model may misestimate FMC volume by ignoring FMC thickness variations within individual ore blocks. Furthermore, simulated block metal grades, thicknesses and densities are based on FMC occurrences from other regions, assuming geological similarity that may not exist. The use of interpolation from a regular drill grid could also fail to capture spatial variability of these parameters, while assuming fixed

Table 6. Resulting design requirements for an FMC mining system.

Design parameter	Type	Limit	Recommended value	Optimal value	Unit
Depth range	Quantitative	–	2500	>2500	m
Mineable slope angle	Quantitative	5	15	22.5	°
Mineable crust thickness	Quantitative	2.5	<10	<5	cm
Mining efficiency	Quantitative	40	80	–	%
Mining rate	Quantitative	0.6	0.9	1.5	Million tons per annum
System availability	Quantitative	45	75	–	%
Ore dilution	Quantitative	60	<30	–	%
Mobility	Qualitative	Needs to be able to relocate several hundreds of meters across the mine site.			
Traction	Qualitative	Needs to operate mainly on hard substrate.			

FMC and substrate water content overlook porosity-dependent variations. Consequently, the hypothetical model may not accurately represent the volume and tonnage of an actual FMC deposit, but it remains a useful tool for better understanding the most important design requirements.

The calculation of dry block mass ($mass_{dry,\,crust,\,block}$) assumes a fixed FMC water content, yet water content likely varies between blocks, affecting recoverable metal quantities. Uncertainty also arises from metal losses during mining ($\eta_{mining,\,block}$), beneficiation ($\eta_{beneficiation,\,crust}$), and metallurgy ($\eta_{metallurgy,\,i}$)—parameters derived from SMS and PMN mining that may not accurately reflect FMC mining efficiencies. Assuming full conversion of remaining metals into metallurgical products could overestimate yields, and the presumed similarity between FMC and PMN further complicates metallurgical performance estimates. The impact of variable feed grade and feed rate on downstream processing remains unaddressed, emphasizing the need for future FMC EBMs to incorporate variable recoveries. Price estimates ($price_{product,\,i}$) based on average market prices of analogous commodities may not represent FMC-derived products. Collectively, these factors introduce significant uncertainty in revenue estimates for each ore block.

The wet mined mass ($mass_{mined,\,wet,\,block}$) is calculated using a fixed dilution rate, although this parameter likely varies with substrate types (Morgan 2006). By simplifying the substrate to a uniform material and overlooking rock properties such compressive strength, mining time estimates and thus block offshore costs ($Cost_{offshore,\,block}$) become uncertain. The onshore cost per block ($Cost_{onshore,\,block}$) is also uncertain, as variations in substrate composition and proportion in the ROM can affect beneficiation costs and metallurgical efficiency. The assumption of complete ROM dewatering during beneficiation may not be feasible, potentially skewing estimates of crust ($mass_{crust,\,beneficiation}$) and substrate mass ($mass_{substrate,\,beneficiation}$) after beneficiation. Omission of waste treatment costs might further result in an underestimation of onshore processing costs.

5.8. Framework applicability

Despite many uncertainties in the geological block model and EBM, the framework for evaluating design requirements remains robust and adaptable. As more reliable data becomes available, the framework can be refined and validated for future assessments. Although the current CMS design requirements are contingent on the illustrated deposit conditions, the framework is applicable once actual sampling data and closely spaced drilling data allow for establishing empirical variograms for FMC interpolation. Moreover, this framework can be adapted to other deep-sea mineral deposits. Future studies should incorporate economies of scale to derive more realistic and practical results.

6. Conclusions

This study explored the value-generating design requirements for a CMS using a hypothetical EBM. While few conceptual CMS designs exist in the literature, the specific design requirements for these studies remain largely unexplored, representing a critical research gap. To address this, EBMs were developed using geological and economic data from existing literature, supplemented by key assumptions. A sensitivity study on the EBMs identified the most crucial design parameters and provided indications on the economic considerations of an FMC mining operation.

Among the identified design requirements, mining system efficiency has the greatest impact on deposit value. Enhancing mining efficiency could increase deposit value for the present case by approximately 11 million USD. The choice of metallurgical processing route significantly affect revenue, with cobalt and manganese emerging as primary contributors, positioning FMC mining as a manganese-cobalt-driven venture. The results demonstrate that CMS design requirements depend on the characteristics of the EBM, which, in turn, depend on the geological characteristics of the mineralization. In the illustrated case, FMC mining on seamount flanks requires specialized mining machines with enhanced mobility and long-distance relocation capabilities to efficiently extract scattered high-value ore zones from steep slopes.

Overall, the proposed framework effectively assessed the impact of key engineering parameters on deposit value, highlighting the critical role EBMs can play in guiding DSM system design. These insights provide a solid foundation for future CMS design studies.

Notes

1. It is assumed that the FMC mining machine extracts the entire thickness of an FMC block down to the substrate, yielding a fixed dilution ratio. The term mining machine is used to denote the part of the mining system responsible for extraction.
2. The mined mixture of ore and substrate prior to any type of treatment.
3. For simplification, dewatering during beneficiation is assumed to remove both saturation and sorbed water from the ROM.

Acknowledgments

We sincerely thank the two anonymous reviewers for their valuable comments, which significantly improved the manuscript. We also extend our gratitude to Dr. Per Olaf Brett (Ulstein International AS and NTNU) for his insightful feedback and discussions. The ISA is acknowledged for providing shapefiles and granting permission for their use; the Cook Islands Seabed Minerals Authority is acknowledged for granting permission to reproduce their shapefiles. Contains data supplied by permission of the Natural Environment Research Council 2023. Contains data under the Norwegian license for Open Government data (NLOD) distributed by the Norwegian Offshore Directorate (SODIR).

Authors' contribution

R. S.: Conceptualization, Methodology, Software, Validation, Investigation, Writing—Original Draft, Writing—Review and Editing. M. L.: Conceptualization, Methodology, Validation, Writing—Review and Editing, Supervision. S. L. E.: Conceptualization, Resources, Project administration, Writing—Review and Editing, Supervision.

Disclosure statement

The authors report there are no competing interests to declare. The funders were not involved in the study's design, data collection, analysis, or interpretation, nor in the writing of the manuscript, the decision to submit for publication, or the selection of the scientific journal. Additionally, the authors declare that they have no known competing financial interests or personal relationships that could have influenced the work reported in this article.

Funding

This work was funded by the Norwegian Ministry of Education and Research as part of the Triple Deep project, which is a component of NTNU's Interdsciplinary Sustainability Initiative.

Data availability statement

The principal data supporting this study are included within this article, and supporting datasets are available at: https://doi.org/10.17632/j9mpp8svbm.1.

References

Adamczyk, K., K. Mizell, D. Payan, N. O. Dominguez, L. Oliva, and A. Gartman. 2023. Marine Mineral Geochemical Data—Part One: Pacific Ocean USGS-Affiliated Historical Data (dataset). U.S. Geological Survey Data Release. https://doi.org/10.5066/P9GD1JKB.

Agarwal, J. C., N. Beecher, D. S. Davies, G. L. Hubred, V. K. Kakari, and R. N. Kust. 1976. Processing of Ocean Nodules: A Technical and Economic Review. *Journal of the Minerals Metals and Materials Society* 28 (4): 24–31. https://doi.org/10.1007/BF03354283.

Allen, J. P., H. L. Abercrombie, and D. A. Rice. 1991. Leaching and Recovery of Metals from Cobalt-Rich Manganese Ocean Crust. *Mining, Metallurgy & Exploration* 8 (2): 97–104. https://doi.org/10.1007/BF03402939.

AMC. 2021. Technical Report Summary – Initial Assessment of the NORI Property, Clarion-Clipperton Zone, for Deep Green Metals Inc. AMC Consultants Pty Ltd. https://metals.co/wp-content/uploads/2022/03/01.05-NORI-D-Initial-Assessment-US-SK-1300-by-AMC-March-2021.pdf

Amon, D. J., S. Gollner, T. Morato, C. R. Smith, C. Chen, S. Christiansen, B. Currie, et al. 2022. Assessment of Scientific Gaps Related to the Effective Environmental Management of Deep-Seabed Mining. *Marine Policy* 138: 105006. https://doi.org/10.1016/j.marpol.2022.105006.

Barnes, R. J. 1991. The Variogram Sill and the Sample Variance. *Mathematical Geology* 23 (4): 673–678. https://doi.org/10.1007/BF02065813.

Benchmark Mineral Intelligence. 2023. Life Cycle Assessment for TMC's NORI-D Polymetallic Nodule Project and Comparison to Key Land-Based Routes for Producing Nickel, Cobalt, and Copper. The Metals Company. https://metals.co/wp-content/uploads/2023/03/TMC_NORI-D_LCA_Final_Report_March2023.pdf

BGR. 2018. "Environmental Impact Assessment for the Testing of a Pre-Protoype Manganese Nodule Collector Vehicle in the Eastern German License Area (Clarion-Clipperton Zone) in the Framework of the European JPI-O MiningImpact 2 Research Project." https://www.isa.org.jm/wp-content/uploads/2022/04/EIA_BGR_0.pdf.

Boulby, M. N., V. Canaguier, and J. R. Donald. 2023. Using Polymetallic Nodules to Innovate Manganese Markets: A New Manganese Feed for SiMn Alloy Production. *Proceedings of the 61st Conference of Metallurgists, COM 2022*, 993–1005. https://doi.org/10.1007/978-3-031-17425-4_108.

Callies, D. L., and C. J. Johnson. 1989. Legal, Business and Economic Aspects of Cobalt-Rich Manganese Crust Mining and Processing in Republic of the Marshall Islands [Unpublished report]. Honolulu, Hawaii: University of Hawaii at Manoa.

Cathles, L. M., and A. C. Simon. 2024. Copper Mining and Vehicle Electrification—A Report by the International Energy Forum. International Energy Forum (IEF). https://www.ief.org/focus/ief-reports/copper-mining-and-vehicle-electrification

CRIRSCO. 2024. International Reporting Template for the Public Reporting of Exploration Targets, Exploration Results, Mineral Resources and Mineral Reserves. Committee for Mineral Reserves International Reporting Standards. https://crirsco.com/the-international-reporting-template/

Cruickshank, M. H., and R. C. Paul. 1986. Characterization of Seabed Rocks for Mine Planning in the EEZ. Paper presented at the Offshore Technology Conference (OTC), Houston, TX, May 1986. https://doi.org/10.4043/5236-MS.

Dames & Moore, and EIC Corporation. 1977. Description of Manganese Nodule Processing Activities for Environmental Studies. *Volume III: Processing Systems Technical Analyses*. Rockville, MD: United States Department of Commerce, National Oceanic and Atmospheric Administration, Office of Marine Minerals.

Das, R. P., and S. Anand. 2017. Metallurgical Processing of Polymetallic Ocean Nodules. In *Deep-Sea Mining Resource Potential, Technical and Environmental Considerations*, ed. R. Sharma, 365–394. Cham: Springer International Publishing. https://doi.org/10.1007/978-3-319-52557-0_12.

Du, D. 2020. Relationships between Slope Gradients and Types of Deposition on the Four Guyots *(Version V3)*. Mendeley Data. https://doi.org/10.17632/g83593d5jc.3.

Du, D., X. Ren, S. Yan, X. Shi, Y. Liu, and G. He. 2017. An Integrated Method for the Quantitative Evaluation of Mineral Resources of Cobalt-Rich Crusts on Seamounts. *Ore Geology Reviews* 84: 174–184. https://doi.org/10.1016/j.oregeorev.2017.01.011.

Du, D., S. Yan, F. Yang, Z. Zhu, Q. Song, and G. Yang. 2018. Kriging Interpolation for Evaluating the Mineral Resources of Cobalt-Rich Crusts on Magellan Seamounts. *Minerals* 8 (9): 374. https://doi.org/10.3390/min8090374.

Du, D., S. Yan, G. Yang, F. Shi, Z. Zhu, Q. Song, F. Yang, Y. Cui, and X. Shi. 2020. Depositional Patterns Constrained by Slope Topography Changes on Seamounts. *Scientific Reports* 10 (1): 20534. https://doi.org/10.1038/s41598-020-77573-2.

Dubiński, J., and A. Koteras. 2023. Mining and Minerals. In *The Palgrave Handbook of Global Sustainability*, ed. R. Brinkmann, 605–630. Cham: Springer International Publishing. https://doi.org/10.1007/978-3-031-01949-4_43.

Ebrahimi, Anoush. 2013. "An Attempt to Standardize the Estimation of Dilution Factor for Open Pit Mining Projects." *Canadian Institute of Mining, Metallurgy and Petroleum, 2013*.

Ellefmo, S. L. 2022. Conceptual 3D Modeling and Direct Block Scheduling of a Massive Seafloor Sulfide Occurrence. In *Perspectives on Deep-Sea Mining*, ed. R. Sharma, 465–496. Cham: Springer International Publishing. https://doi.org/10.1007/978-3-030-87982-2_16.

EQR. 2023. Mt Carbine Bankable Feasibility Study – 2023 Economic Update. https://www.eqresources.com.au/pdf/Operating_Cost_Estimate.pdf

ESRI. 2014. World Ocean Base [Basemap] [Map]. https://services.arcgisonline.com/ArcGIS/rest/services/Ocean/World_Ocean_Base/MapServer

ETC. 2023. Materials and Resource Requirements for the Energy Transition (The Barriers to Clean Electrification Series). Energy Transitions Commission. https://www.energy-transitions.org/publications/material-and-resource-energy-transition#download-form

European Commission: Directorate-General for Internal Market, Industry, Entrepreneurship and SMEs, Grohol, M., and Veeh, C. 2023. *Study on the Critical Raw Materials for the EU 2023—Final Report*. Luxembourg: Publications Office of the European Union. https://doi.org/10.2873/725585.

Flanders Marine Institute. 2023. Maritime Boundaries Geodatabase: Maritime Boundaries and Exclusive Economic Zones (200NM) (Version 12) (dataset). https://doi.org/10.14284/632.

Flanders Marine Institute. 2024. Maritime Boundaries Geodatabase: Extended Continental Shelves (Version 2) (dataset). https://doi.org/10.14284/697.

Fouche, G., and N. Adomaitis. 2024. Norway Stops Deep-Sea Mining, for Now. Reuters. https://www.reuters.com/world/europe/norway-stop-deep-sea-mining-says-party-supporting-minority-government-2024-12-01/

Fritz, Benjamin, Pia Heidak, Jürgen Vasters, Thomas Kuhn, Gudrun Franken, and Mario Schmidt. 2023. "Life Cycle Impact on Climate Change Caused by Metal Production from Deep Sea Manganese Nodules versus Land-Based Deposits." *Resources, Conservation and Recycling* 193 (June):106976. https://doi.org/10.1016/j.resconrec.2023.106976.

Fuerstenau, D. W., and K. N. Han. 1983. Metallurgy and Processing of Marine Manganese Nodules. *Mineral Processing and Extractive Metallurgy Review* 1 (1–2): 1–83. https://doi.org/10.1080/08827508308952589.

Goto, K., T. Yamazaki, R. Arai, and N. Nakatani. 2009. Effects of Microtopography on Mining Possibility of Cobalt-Rich Manganese Crusts. In *Proceedings of The Eighth (2009) ISOPE Ocean Mining Symposium*, 239–245.

Goto, K., T. Yamazaki, N. Nakatani, and R. Arai. 2010. Preliminary Economic Feasibility Analysis of Cobalt-Rich Manganese Crust Mining for Rare Metal Recovery. In *Proceedings of the ASME 2010 29th International Conference on Ocean, Offshore and Arctic Engineering*, 29–34. https://doi.org/10.1115/OMAE2010-20243.

Halbach, P., A. Jahn, and G. Cherkashov. 2017. Marine Co-Rich Ferromanganese Crust Deposits: Description and Formation, Occurrences and Distribution, Estimated World-Wide Resources. In *Deep-Sea Mining: Resource Potential, Technical and Environmental Considerations*, ed. R. Sharma Cham: Springer International Publishing. https://doi.org/10.1007/978-3-319-52557-0.

Halbach, P., and F. T. Manheim. 1984. Potential of Cobalt and Other Metals in Ferromanganese Crusts on Seamounts of the Central Pacific Basin. *Marine Mining* 4 (4): 319–336. https://pubs.usgs.gov/publication/70207304.

Halbach, P., C. D. Sattler, F. Teichmann, and M. Wahsner. 1987. Characterization of Co-Rich Ferromanganese Crust Fields within the Johnston Island EEZ (Central Pacific). In *Proceedings of Oceans '87. The Ocean—an International Workplace*, 1015–1020. https://doi.org/10.1109/OCEANS.1987.1160702.

Halkyard, J. 1985. Technology for Mining Cobalt Rich Manganese Crusts from Seamounts. In *Proceedings of Oceans '85—Ocean Engineering and the Environment*, 352–374. https://doi.org/10.1109/OCEANS.1985.1160238.

Halvorsen, T. 2022. System for Mining Subsea Metallic Crusts (Patent No. WO/2022/191712). https://patentscope.wipo.int/search/en/detail.jsf?docId=WO2022191712&_cid=P20-M7LWAR-07036-1

Hardy, R. L. 1971. Multiquadric Equations of Topography and Other Irregular Surfaces. *Journal of Geophysical Research* 76 (8): 1905–1915. https://doi.org/10.1029/JB076i008p01905.

Harris, C. R., K. J. Millman, S. J. Van Der Walt, R. Gommers, P. Virtanen, D. Cournapeau, E. Wieser, et al. 2020. Array Programming with NumPy. *Nature* 585 (7825): 357–362. https://doi.org/10.1038/s41586-020-2649-2.

Hartman, H. L., and J. M. Mutmansky. 2002. *Introductory Mining Engineering*. 2nd ed. New York: John Wiley & Sons.

Haynes, B. W., S. L. Law, and R. Maeda. 1983. *Updated Process Flowsheets for Manganese Nodule Processing (Information Circular 8924)*. Washington, DC: U.S. Department of the Interior, Bureau of Mines, 1–100.

Hein, J. R. 2004. Cobalt-Rich Ferromanganese Crusts: Global Distribution, Composition, Origin and Research Activities. In *Workshop on Minerals Other than Polymetallic Nodules of the International Seabed Area: Proceedings of the International Seabed Authority Workshop Held on 26–30 June 2000 in Kingston, Jamaica*, 188–272.

Hein, J. R. 2006. Prospecting and Exploration for Cobalt-Rich Ferromanganese Crusts Deposits in the Area. In Mining Cobalt-Rich Ferromanganese Crusts and Polymetallic Sulphides Deposits: Technological and Economic Considerations. *Proceedings of the International Seabed Authority's Workshop Held in Kingston, Jamaica, 31* July–4 August 2006, 102–130.

Hein, J. R., T. A. Conrad, and R. E. Dunham. 2009. Seamount Characteristics and Mine-Site Model Applied to Exploration- and Mining-Lease-Block Selection for Cobalt-Rich Ferromanganese Crusts. *Marine Georesources & Geotechnology* 27 (2): 160–176. https://doi.org/10.1080/10641190902852485.

Hein, J. R., T. A. Conrad, M. Frank, M. Christl, and W. W. Sager. 2012. Copper-Nickel-Rich, Amalgamated Ferromanganese Crust-Nodule Deposits from Shatsky Rise, NW Pacific. *Geochemistry*, Geophysics, Geosystems, 13(10): 1–23. https://doi.org/10.1029/2012GC004286.

Hein, J. R., A. Koschinsk, M. Bau, F. T. Manheim, J. K. Kang, and L. Roberts. 2017. Cobalt-Rich Ferromanganese Crusts in the Pacific. In *Handbook of Marine Mineral Deposits*, 1st ed., ed. D. S. Cronan, 239–279. London: Routledge. https://doi.org/10.1201/9780203752760-9.

Hein, J. R., and A. Koschinsky. 2014. Deep-Ocean Ferromanganese Crusts and Nodules. In *Treatise on Geochemistry*, 273–291. Amsterdam: Elsevier. https://doi.org/10.1016/B978-0-08-095975-7.01111-6.

Hein, J. R., A. Koschinsky, M. Bau, F. T. Manheim, J. K. Kang, and L. Roberts. 2000. Cobalt-Rich Ferromanganese Crusts in the Pacific. In *Handbook of Marine Minerals*, ed. D. S. Cronan, 1st ed., 239–279. Boca Raton, FL: CRC Press. https://doi.org/10.1201/9780203752760-9.

Hein, J. R., A. Koschinsky, and A. N. Halliday. 2003. Global Occurrence of Tellurium-Rich Ferromanganese Crusts and a Model for the Enrichment of Tellurium. *Geochimica et Cosmochimica Acta* 67 (6): 1117–1127. https://doi.org/10.1016/S0016-7037(02)01279-6.

Hein, J. R., A. Koschinsky, and T. Kuhn. 2020. Deep-Ocean Polymetallic Nodules as a Resource for Critical Materials. *Nature Reviews Earth & Environment* 1 (3): 158–169. https://doi.org/10.1038/s43017-020-0027-0.

Hein, J. R., F. T. Manheim, W. C. Schwab, A. S. Davis, C. L. Daniel, R. M. Bouse, L. A. Morgenson, et al. 1985. Geological and Geochemical Data for Seamounts and Associated Ferromanganese Crusts in and near the Hawaiian, Johnston Island, and Palmyra Island Exclusive Economic Zones (U.S. Geological Survey Open File Report Nos. 85–292). U.S. Department of Interior. https://pubs.usgs.gov/of/1985/0292/report.pdf

Hein, J. R., K. Mizell, A. Koschinsky, and T. A. Conrad. 2013. Deep-Ocean Mineral Deposits as a Source of Critical Metals for High- and Green-Technology Applications: Comparison with Land-Based Resources. *Ore Geology Reviews* 51: 1–14. https://doi.org/10.1016/j.oregeorev.2012.12.001.

Hein, J. R., J. W. Moon, K. Y. Lee, K. H. Kim, L. Roberts, M. Burrows, S. H. Park, et al. 1998. Composition of Co-Rich Ferromanganese Crusts and Substrate Rocks from the Marshall Islands, Cruise KODOS 97-4 (U.S. Geological Survey Open File Report Nos. 98–375). U.S. Department of Interior. https://pubs.usgs.gov/of/1998/0375/report.pdf

Hino, H., and A. Usui. 2022. Regional and Fine-Scale Variability in Composition and Structure of Hydrogenetic Ferromanganese Crusts: Geological Characterization of 25 Drill Cores from the Marcus-Wake Seamounts. *Marine Georesources & Geotechnology* 40 (4): 415–437. https://doi.org/10.1080/1064119X.2021.1904066.

Hino, H., A. Usui, H. Morozumi, A. Suzuki, K. Kurihara, T. Suzuki, and N. Okamoto. 2024. Geological Characterization and Controlling Factors of Small-Scale Variations in the Cobalt-Rich Ferromanganese Crust Deposits. *Marine Georesources & Geotechnology* 42 (8): 1063–1074. https://doi.org/10.1080/1064119X.2023.2249875.

Hirt, W. C., D. A. Rice, and M. B. Shirts. 1991. Flotation of Cobalt-Rich Ferromanganese Crust from the Pacific Ocean. *Minerals Engineering* 4 (5–6): 535–551. https://doi.org/10.1016/0892-6875(91)90001-C.

Hodkinson, R. A., and D. S. Cronan. 1991. Regional and Depth Variability in the Composition of Cobalt-Rich Ferromanganese

Crusts from the SOPAC Area and Adjacent Parts of the Central Equatorial Pacific. *Marine Geology* 98 (2–4): 437–447. https://doi.org/10.1016/0025-3227(91)90115-K.

Howard, P., G. Parker, N. Jenner, and T. Holland. 2020. *An Assessment of the Risks and Impacts of Seabed Mining on Marine Ecosystems*. Cambridge, UK: Fauna & Flora International, 337 https://www.fauna-flora.org/wp-content/uploads/2023/05/FFI_2020_The-risks-impacts-deep-seabed-mining_Report.pdf.

Huang, D., Y. Sun, W. Gao, W. Xu, W. Wang, Y. Zhang, and L. Wang. 2024. Research on Seamount Substrate Classification Method Based on Machine Learning. *Frontiers in Marine Science* 11: 1431688. https://doi.org/10.3389/fmars.2024.1431688.

Hunter, J. D. 2007. Matplotlib: A 2D Graphics Environment. *Computing in Science & Engineering* 9 (3): 90–95. https://doi.org/10.1109/MCSE.2007.55.

Hwang, G., Y. Ko, S. Yang, and W. Kim. 2024. Resource Abundance of Cobalt-Rich Ferromanganese Crusts in the KC-8 Seamount, West Pacific. *Frontiers in Earth Science* 12: 1495673. https://doi.org/10.3389/feart.2024.1495673.

IEA. 2024a. Global Critical Minerals Outlook 2024. International Energy Agency. https://www.iea.org/reports/global-critical-minerals-outlook-2024

IEA. 2024b. Global EV Outlook 2024 Moving towards Increased Affordability. International Energy Agency. https://www.iea.org/reports/global-ev-outlook-2024/trends-in-electric-vehicle-batteries

ISA. 2012. Decision of the Assembly of the International Seabed Authority Relating to the Regulations on Prospecting and Exploration for Cobalt-Rich Ferromanganese Crusts in the Area. International Seabed Authority. https://www.isa.org.jm/wp-content/uploads/2022/04/isba-18a-11_0.pdf

ISA. 2024a. Shapefiles (dataset). International Seabed Authority. https://www.isa.org.jm/exploration-contracts/maps/

ISA. 2024b. Status of Exploration Activities in the Area. International Seabed Authority. https://www.isa.org.jm/wp-content/uploads/2024/07/ISA_Status_of_exploration_activities_June_2024.pdf

Ito, M., M. Tsunekawa, E. Yamaguchi, K. Sekimura, K. Kashiwaya, K. Hori, and N. Hiroyoshi. 2008. Estimation of Degree of Liberation in a Coarse Crushed Product of Cobalt-Rich Ferromanganese Crust/Nodules and Its Gravity Separation. *International Journal of Mineral Processing* 87 (3–4): 100–105. https://doi.org/10.1016/j.minpro.2008.02.005.

Jiang, K., L. Y. Feng, W. Jiang, and X. X. Jiang. 2016. Study on the Reductive Leaching of the Seabed Co-Mn Polymetallic Ore with Co and Ammonia. In Proceedings of ALTA 2016 Nickel-Cobalt-Copper-Sessions, 23–25 May 2016, *Perth, Australia*, 35–46. https://d3e2i5nuh73s15.cloudfront.net/wp-content/uploads/2018/03/ALTA-2016-NCC-Proceedings.pdf.

Josso, P., and A. Hall. 2022. Random Forest Model Output Prediction Raster for the Occurrence of Fe-Mn in the World Oceans (dataset). NERC, EDS, National Geoscience Data Centre. https://doi.org/10.5285/4c8419b9-5ee4-4db4-b279-18d3ec75c3c4.

Josso, P., A. Hall, C. Williams, T. Le Bas, P. Lusty, and B. Murton. 2023. Application of Random-Forest Machine Learning Algorithm for Mineral Predictive Mapping of Fe-Mn Crusts in the World Ocean. *Ore Geology Reviews* 162: 105671. https://doi.org/10.1016/j.oregeorev.2023.105671.

Karakitsos, E., and L. Varnavides. 2014. *Maritime Economics: A Macroeconomic Approach*. 1st ed. London: Palgrave Macmillan. https://doi.org/10.1057/9781137383419.

Kirchain, R., R. Roth, F. R. Field, C. Muñoz-Royo, and T. Peacock. 2019. *Report to the International Seabed Authority on the Development of an Economic Model and System of Payments for the Exploitation of Polymetallic Nodules in the Area*. Cambridge, MA: Massachusetts Institute of Technology (MIT), MIT Materials Systems Laboratory, 77.

Konstantinova, N., G. Cherkashov, J. R. Hein, J. Mirão, L. Dias, P. Madureira, V. Kuznetsov, and F. Maksimov. 2017. Composition and Characteristics of the Ferromanganese Crusts from the Western Arctic Ocean. *Ore Geology Reviews* 87: 88–99. https://doi.org/10.1016/j.oregeorev.2016.09.011.

Koschinsky, A., and P. Halbach. 1995. Sequential Leaching of Marine Ferromanganese Precipitates: Genetic Implications. *Geochimica et Cosmochimica Acta* 59 (24): 5113–5132. https://doi.org/10.1016/0016-7037(95)00358-4.

Lesage, M. 2019. A Framework for Evaluating Deep Sea Mining Systems for Seafloor Massive Sulphides Deposits. PhD diss., NTNU. https://hdl.handle.net/11250/2677911

Lesage, M., C. Juliani, and S. L. Ellefmo. 2018. Economic Block Model Development for Mining Seafloor Massive Sulfides. *Minerals* 8 (10): 468. https://doi.org/10.3390/min8100468.

Lipton, I., E. Gleeson, and P. Munro. 2018. Preliminary Economic Assessment of the Solwara Project, Bismarck Sea, PNG. AMC Consultants Pty Ltd. https://minedocs.com/11/Solwara_1_PEA_02272018.pdf

Lipton, I., M. J. Nimmo, and J. M. Parianos. 2016. NI 43-101 Technical Report: TOML Clarion Clipperton Zone Project, Pacific Ocean. AMC Consultants Pty Ltd. https://doi.org/10.13140/RG.2.2.23742.08000.

Little, A. D. 1984. *Technical and Cost Analyses of Manganese Nodule Processing Techniques and Their Significant Variations*. Washington, DC: U.S. Department of Commerce, National Oceanic & Athomspheric Administration (NOAA), Ocean Minerals and Energy.

Machida, S., K. Fujinaga, T. Ishii, K. Nakamura, N. Hirano, and Y. Kato. 2016. Geology and Geochemistry of Ferromanganese Nodules in the Japanese Exclusive Economic Zone around Minamitorishima Island. *Geochemical Journal* 50 (6): 539–555. https://doi.org/10.2343/geochemj.2.0419.

Madureira, P., H. Brekke, G. Cherkashov, and M. Rovere. 2016. Exploration of Polymetallic Nodules in the Area: Reporting Practices, Data Management and Transparency. *Marine Policy* 70: 101–107. https://doi.org/10.1016/j.marpol.2016.04.051.

Malnic, J. 2008. The Direct Nickel Process for Treating Seafloor Ferromanganese Deposits. In Polymetallic Nodule Mining Technology: Current Trends and Challenges Ahead. Proceedings of the Workshop Jointly Organized by The International Seabed Authority and the National Institute of Ocean Technology, Chennai [Ministry of Earth Sciences], Government of India, 18–22 February 2008, 231–236. https://www.isa.org.jm/wp-content/uploads/2023/10/chennai-19sept-final.pdf.

Manheim, F. T., and C. M. Lane-Botswick. 1989. Chemical Composition of Ferromanganese Crusts in the World Ocean: A Review and Comprehensive Database (Open-File Report *89-020)*.

McKinney, W. 2010. Data Structures for Statistical Computing in Python. In *Proceedings of the 9th Python in Science Conference, Austin, TX*. https://doi.org/10.25080/Majora-92bf1922-00a.

Miller, K. A., K. Brigden, D. Santillo, D. Currie, P. Johnston, and K. F. Thompson. 2021. Challenging the Need for Deep Seabed Mining from the Perspective of Metal Demand, Biodiversity, Ecosystems Services, and Benefit Sharing. *Frontiers in Marine Science* 8: 706161. https://doi.org/10.3389/fmars.2021.706161.

Mittal, N. K., and P. K. Sen. 2003. India's First Medium Scale Demonstration Plant for Treating Poly-Metallic Nodules. *Minerals Engineering* 16 (9): 865–868. https://doi.org/10.1016/S0892-6875(03)00204-8.

Mizell, K., and J. R. Hein. 2018. Ferromanganese Crusts and Nodules: Rocks That Grow. In *Encyclopedia of Geochemistry: A Comprehensive Reference Source on the Chemistry of the Earth*, ed. W. M. White, 1–5. Cham: Springer International Publishing. https://doi.org/10.1007/978-3-319-39312-4.

Mizell, K., J. R. Hein, M. Au, and A. Gartman. 2022. Estimates of Metals Contained in Abyssal Manganese Nodules and Ferromanganese Crusts in the Global Ocean Based on Regional Variations and Genetic Types of Nodules. In *Perspectives on Deep-Sea Mining: Sustainability, Technology, Environmental Policy and Management*, ed. R. Sharma. Cham: Springer International Publishing. https://doi.org/10.1007/978-3-030-87982-2.

Morgan, C. 2006. Mining Development Scenario Summary (Cobalt-Rich Ferromanganese Crusts Deposits). In *Mining Cobalt-Rich Ferromanganese Crusts and Polymetallic Sulphides Deposits:*

Technological and Economic Considerations. Proceedings of the International Seabed Authority's Workshop Held in Kingston, Jamaica, 31 July–4 August 2006, 131–207. https://www.isa.org.jm/wp-content/uploads/2022/08/2006sulpcrusts-web_0.pdf.

Neettiyath, U., B. Thornton, H. Sugimatsu, T. Sunaga, J. Sakamoto, and H. Hino. 2022. Automatic Detection of Buried Mn-Crust Layers Using a Sub-Bottom Acoustic Probe from AUV Based Surveys. OCEANS 2022 - Chennai, 1–7. https://doi.org/10.1109/oceanschennai45887.2022.9775260.

NOAA. 2023. NOAA National Centers for Environmental Information, 2004: Multibeam Bathymetry Database (MBBDB) (dataset). NOAA National Centers for Environmental Information. https://doi.org/10.7289/V56T0JN.

Novikov, G. V., S. V. Yashina, M. E. Mel'nikov, I. V. Vikent'ev, and O. Yu Bogdanova. 2014. Nature of Co-Bearing Ferromanganese Crusts of the Magellan Seamounts (Pacific Ocean): Communication 2. Ion Exchange Properties of Ore Minerals. *Lithology and Mineral Resources* 49 (2): 138–164. https://doi.org/10.1134/S0024490214020072.

Ochromowicz, K., K. Aasly, and P. Kowalczuk. 2021. Recent Advancements in Metallurgical Processing of Marine Minerals. *Minerals* 11 (12): 1437. https://doi.org/10.3390/min11121437.

Okamoto, N., H. Shibasaki, M. Kobayashi, M. Ito, Y. Konishi, and T. Ooki. 2018. JOGMEC Activities on the R/D of Processing and Metallurgical Technologies for Cobalt-Rich Ferromanganese Crusts. Workshop on Processing Technologies, Metal Recoveries and Economic Feasibility of Deep Sea Mining, *Warsaw, Poland*. https://www.isa.org.jm/wp-content/uploads/2022/12/Jogmec.pdf.

Orita, K., S. Kawano, S. Nakamura, Y. Igarashi, S. Shiokawa, S. Nojiri, Y. Ueyama, and K. Watanabe. 2022. Development of New Mining Machine for Cobalt-Rich Ferromanganese Crust and Achievement of Excavation and Dredging Test on the Deep Seafloor. In *Proceedings of the Thirty-Second (2022) International Ocean and Polar Engineering Conference*.

Pahl, G., W. Beitz, J. Feldhusen, and K. H. Grote. 2007. *Engineering Design: A Systematic Approach*. 3rd ed. Cham: Springer International Publishing. https://doi.org/10.1007/978-1-84628-319-2.

Parianos, J., I. Lipton, and M. Nimmo. 2021. Aspects of Estimation and Reporting of Mineral Resources of Seabed Polymetallic Nodules: A Contemporaneous Case Study. *Minerals* 11 (2): 200. https://doi.org/10.3390/min11020200.

Peacock, T. 2023. The GSR Patania II Expedition: Technical Achievements and Scientific Learning. https://deme-gsr.com/wp-content/uploads/2023/03/2023_March11_GSR_PataniaII_Final_sp_2-page-version-compressed-2.pdf

Pedersen, R. B., B. R. Olseb, T. Barreyre, A. Bjerga, A. Denny, M. H. Eilertsen, I. Fer, et al. 2021. Fagutredning Mineralressurser I Norskehavet—Landskapstrekk, Naturtyper Og Bentiske Økosystemer. Senter For Dyphavsforskning, Universitetet i Bergen. https://www.regjeringen.no/contentassets/a3dd0ce426a14e25abd8b55154f34f20/landskapstrekk-naturtyper-og-bentiske-okosystemer_senter-for-dyphavsforskning-uib.pdf

Petersen, S., A. Krätschell, N. Augustin, J. Jamieson, J. R. Hein, and M. D. Hannington. 2016. News from the Seabed – Geological Characteristics and Resource Potential of Deep-Sea Mineral Resources. *Marine Policy* 70: 175–187. https://doi.org/10.1016/j.marpol.2016.03.012.

Powell, M. J. D. 1992. The Theory of Radial Basis Function Approximation in 1990. In *Advances in Numerical Analysis: Wavelets, Subdivision Algorithms, and Radial Basis Functions*, ed. W. Light. Oxford, UK: Oxford University Press. https://doi.org/10.1093/oso/9780198534396.003.0003.

QGIS.org. 2024. QGIS Geographic Information System. Open Source Geospatial Foundation Project (Computer software). http://qgis.org

Rudenno, V. 2012. *The Mining Valuation Handbook 4e: Mining and Energy Valuation for Investors and Management*. Australia: John Wiley & Sons, Ltd.

Runge, I. C. 1998. Integrating Economics into Mining. In *Mining Economics and Strategy*. Littleton, CO: Society for Mining Engineering, Metallurgy and Exploration, Inc.

SBMA. 2023. The Cook Islands Seabed Minerals Journey. Seabed Minerals Authority. https://static1.squarespace.com/static/5cca30fab2cf793ec6d94096/t/663e5fc61d3e7031d03a00f3/1715363808504/General+CI+Seabed+Mineral+Journey_FINAL+Nov23.pdf

Seequent. n.d. Leapfrog Geo (Computer Software). https://www.seequent.com/products-solutions/leapfrog-geo/

SODIR. 2024. Anbefalte Blokker Til Utlysning på Offentlig Høring, Last Ned, Blokker Til Høring (Shapefiler) (dataset). Sokkeldirektoratet. https://www.sodir.no/fakta/havbunnsmineraler/konsesjonsrunder/1.-konsesjonsrunde/anbefalte-blokker-til-utlysning-pa-offentlig-horing/

Sparenberg, O. 2019. A Historical Perspective on Deep-Sea Mining for Manganese Nodules, 1965–2019. *The Extractive Industries and Society* 6 (3): 842–854. https://doi.org/10.1016/j.exis.2019.04.001.

SPC. 2016. An Assessment of the Costs and Benefits of Mining Deepsea Minerals in the Pacific Island Region: Deep-Sea Mining Cost-Benefit Analysis (No. SPC Technical Report SPC00035; p. 229). Pacific Community (SPC). https://www.sprep.org/attachments/VirLib/Regional/deep-sea-mining-cba-PICs-2016.pdf

SRK Consulting. 2010. Offshore Production System Definition and Cost Study (Nos. SL01-NSG-XSR-RPT-7105–001; p. 275). https://actnowpng.org/sites/default/files/Solwara%201%20Production%20System%20Definition%20and%20Cost%20Study%202010.pdf

Stutt, A. 2019. *Nautilus Minerals Officially Sinks, Shares Still Trading*. MINING.COM. https://www.mining.com/nautilus-minerals-officially-sinks-shares-still-trading/

Svininnikov, A. I. 1994. Physical properties of rocks and sediments from Karin Ridge (Central Equatorial Pacific) and the Bering Sea. In *Data and Results from R.V. Aleksandr Vinogradov Cruises 91-AV-19/1, North Pacific Hydrochemistry Transect; 91-AV-19/2, North Equatorial Pacific Karin Ridge Fe-Mn Crust Studies; and 9l-AV∼19/4, Northwest Pacific and Bering Sea Sediment Geochemistry and Paleoceanographic Studies (U.S. Geological Survey Open File Report 94-230)*, eds. J. R. Hein, A. S. Bychkov, and A. E. Gibbs, 103. Reston, VA: U.S. Department of Interior. https://pubs.usgs.gov/of/1994/0230/report.pdf.

Takahashi, T., M. Ito, N. Hiroyoshi, M. Kameya, and Y. Aoki. 2023. A Fundamental Study on Flotation and Gravity Separation of Cobalt-Rich Ferromanganese Crusts. *Poster presented at the 11th International Flotation Conference (Flotation '23)*. https://www.min-eng.com/flotation23/drafts/posters/takahashi.pdf

Tay, S., R. Browne, and O. Bertoli. 2022. Mineral Resource Estimate for Cook Islands Polymetallic Nodule Field [Map]. Seabed Minerals Authority (SBMA). https://static1.squarespace.com/static/5cca30fab2cf793ec6d94096/t/6581ed3054532131d036f11c/1703013799356/CIMinRscMaprev1.pdf

The Japan Times. 2024. Over 200 Million Metric Tons of Rare Metals Found near Remote Tokyo Island. The Japan Times. https://www.japantimes.co.jp/news/2024/06/22/japan/science-health/tokyo-island-rare-metals-find/

The Pandas Development Team. 2020. *Pandas-Dev/Pandas: Pandas (Computer Software)*. Switzerland: Zenodo. https://doi.org/10.5281/zenodo.3509134.

TMC. 2022. TMC and Allseas Achieve Historic Milestone: Nodules Collected from the Seafloor and Lifted to the Production Vessel Using 4 km Riser During Pilot Trials in the Clarion Clipperton Zone for First Time Since the 1970s. https://investors.metals.co/news-releases/news-release-details/tmc-and-allseas-achieve-historic-milestone-nodules-collected/

TMC. 2024a. TMC & SGS Produce World-First Nickel Sulfate from Deep-Seafloor Polymetallic Nodules. https://investors.metals.co/news-releases/news-release-details/tmc-sgs-produce-world-first-nickel-sulfate-deep-seafloor/

TMC. 2024b. TMC and SGS Produce World-First Cobalt Sulfate from Deep-Seafloor Polymetallic Nodules. https://investors.metals.co/news-releases/news-release-details/tmc-and-sgs-produce-world-first-cobalt-sulfate-deep-seafloor/

TMC. 2025. World First: TMC and PAMCO Achieve a New Nodule Processing Milestone, Unlocking Critical Energy & Steelmaking Materials at Existing Facilities. https://investors.metals.co/news-

releases/news-release-details/world-first-tmc-and-pamco-achieve-new-nodule-processing/

UNEP-WCMC, and IUCN. 2024. Protected Planet: The World Database on Protected Areas (WDPA) and World Database on Other Effective Area-Based Conservation Measures (WD-OECM). Cambridge, UK: UNEP-WCMC and IUCN. www.protectedplanet.net

Usui, A., K. Nishi, H. Sato, Y. Nakasato, B. Thornton, T. Kashiwabara, A. Tokumaru, et al. 2017. Continuous Growth of Hydrogenetic Ferromanganese Crusts since 17 Myr Ago on Takuyo-Daigo Seamount, NW Pacific, at Water Depths of 800–5500 m. *Ore Geology Reviews* 87: 71–87. https://doi.org/10.1016/j.oregeorev.2016.09.032.

Van Nijen, K., S. Van Passel, and D. Squires. 2018. A Stochastic Techno-Economic Assessment of Seabed Mining of Polymetallic Nodules in the Clarion Clipperton Fracture Zone. *Marine Policy* 95: 133–141. https://doi.org/10.1016/j.marpol.2018.02.027.

Vogt, Peter R., and N. Christian Smoot. 1984. "The Geisha Guyots: Multibeam Bathymetry and Morphometric Interpretation." Journal of Geophysical Research: Solid Earth 89 (B13): 11085–107. https://doi.org/10.1029/JB089iB13p11085.

Volkmann, S. E. 2019. Blue Mining—Planning the Mining of Seafloor Manganese Nodules. PhD diss., https://publications.rwth-aachen.de/record/750679/files/750679.pdf

Volkmann, S. E., and F. Lehnen. 2018. Production Key Figures for Planning the Mining of Manganese Nodules. *Marine Georesources & Geotechnology* 36 (3): 360–375. https://doi.org/10.1080/1064119X.2017.1319448.

Washburn, T. W., P. J. Turner, J. M. Durden, D. O. B. Jones, P. Weaver, and C. L. Van Dover. 2019. Ecological Risk Assessment for Deep-Sea Mining. *Ocean & Coastal Management* 176: 24–39. https://doi.org/10.1016/j.ocecoaman.2019.04.014.

Waskom, M. 2021. Seaborn: Statistical Data Visualization. *Journal of Open Source Software* 6 (60): 3021. https://doi.org/10.21105/joss.03021.

Wenzel, J. G. 1987. *Mining Development Scenario for Cobalt-Rich Manganese Crusts in the Exclusive Economic Zones of the Hawaiian Archipelago and Johnston Island*. Hawaii: State of Hawaii, Department of Planning and Economic Development.

Wiltshire, J. C., X. Y. Wen, and D. Yao. 1999. Ferromanganese Crusts near Johnston Island: Geochemistry, Stratigraphy and Economic Potential. *Marine Georesources & Geotechnology* 17 (2–3): 257–270. https://doi.org/10.1080/106411999273936.

Xie, C., M. Chen, L. Wang, C. Agee, S. Yao, J. Zheng, J. Liu, et al. 2022. A Study on the Performance Modeling Method for a Deep-Sea Cobalt-Rich Crust Mining Vehicle. *Minerals* 12 (12): 1521. https://doi.org/10.3390/min12121521.

Xie, C., L. Wang, N. Yang, C. Agee, M. Chen, J. Zheng, J. Liu, et al. 2022. A Compact Design of Underwater Mining Vehicle for the Cobalt-Rich Crust with General Support Vessel Part A: Prototype and Tests. *Journal of Marine Science and Engineering* 10 (2): 135. https://doi.org/10.3390/jmse10020135.

Yamazaki, T., S. H. Park, S. Shimada, and T. Yamamoto. 2002. Development of Technical and Economical Examination Method for Cobalt-Rich Manganese Crusts. *Proceedings of The Twelfth (2002) International Offshore and Polar Engineering Conference Kitakyushu*, Japan, *26–31* May, 2002, 454–461.

Yamazaki, T., and R. Sharma. 1998. Distribution Characteristics of co-Rich Manganese Deposits on a Seamount in the Central Pacific Ocean. *Marine Georesources & Geotechnology* 16 (4): 283–305. https://doi.org/10.1080/10641199809379973.

Yeo, I. A., S. A. Howarth, J. Spearman, A. Cooper, N. Crossouard, J. Taylor, M. Turnbull, and B. J. Murton. 2019. Distribution of and Hydrographic Controls on Ferromanganese Crusts: Tropic Seamount, Atlantic. *Ore Geology Reviews* 114: 103131. https://doi.org/10.1016/j.oregeorev.2019.103131.

Zhao, B., Z. Wei, Y. Yang, G. He, H. Zhang, and W. Ma. 2020. Sedimentary Characteristics and the Implications of Cobalt-Rich Crusts Resources at Caiwei Guyot in the Western Pacific Ocean. *Marine Georesources & Geotechnology* 38 (9): 1037–1045. https://doi.org/10.1080/1064119X.2019.1648615.

Appendix A

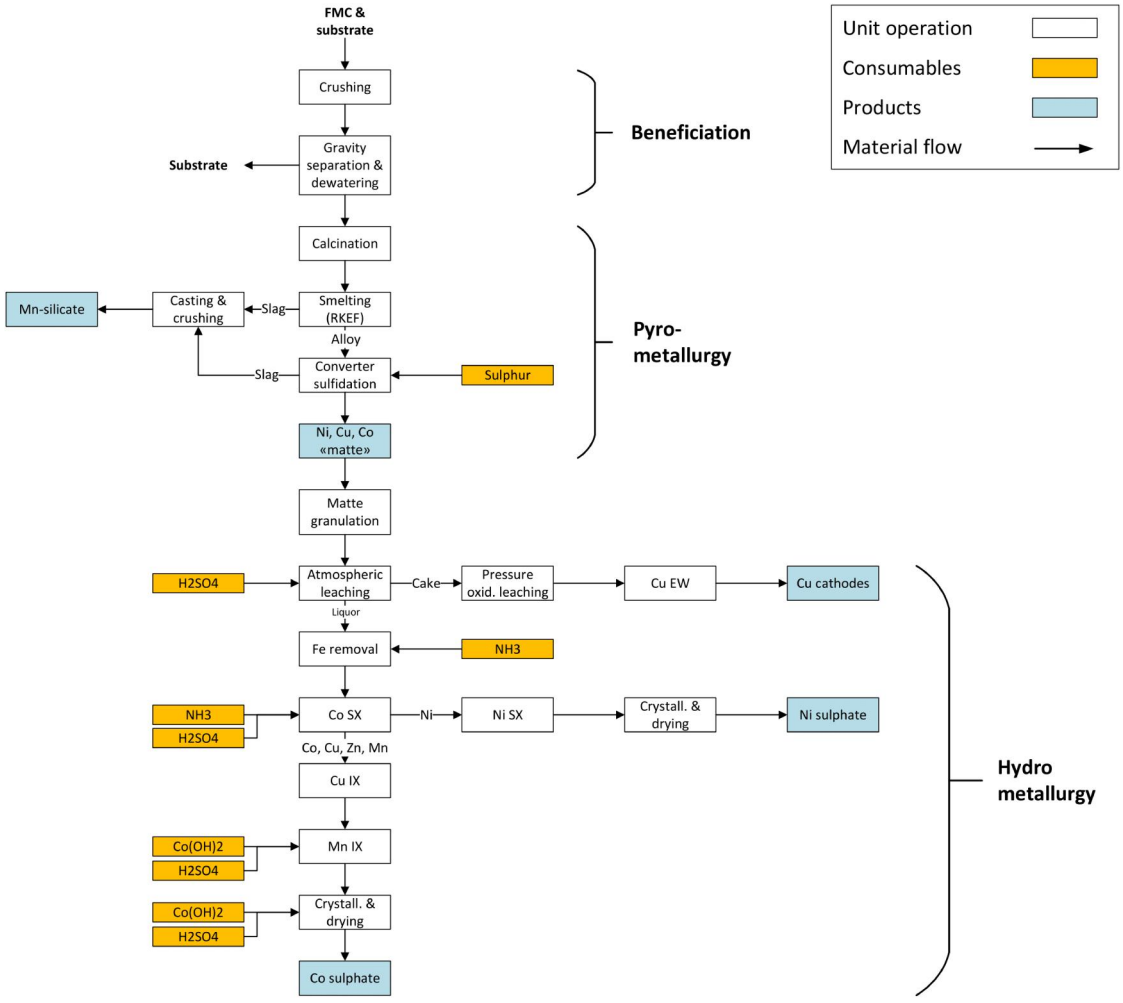

Figure A1. Flowchart of the selected processing route, adapted from TMC's pyro-hydrometallurgical process for PMN. The modified process includes an added crushing and gravity separation (jig) step to remove co-extracted substrate. The process is assumed to generate no significant waste, as pyrometallurgical slag is largely converted to Mn silicate. RKEF = Rotary Kiln–Electric Furnace. Based on AMC (2021) and Benchmark Mineral Intelligence (2023).

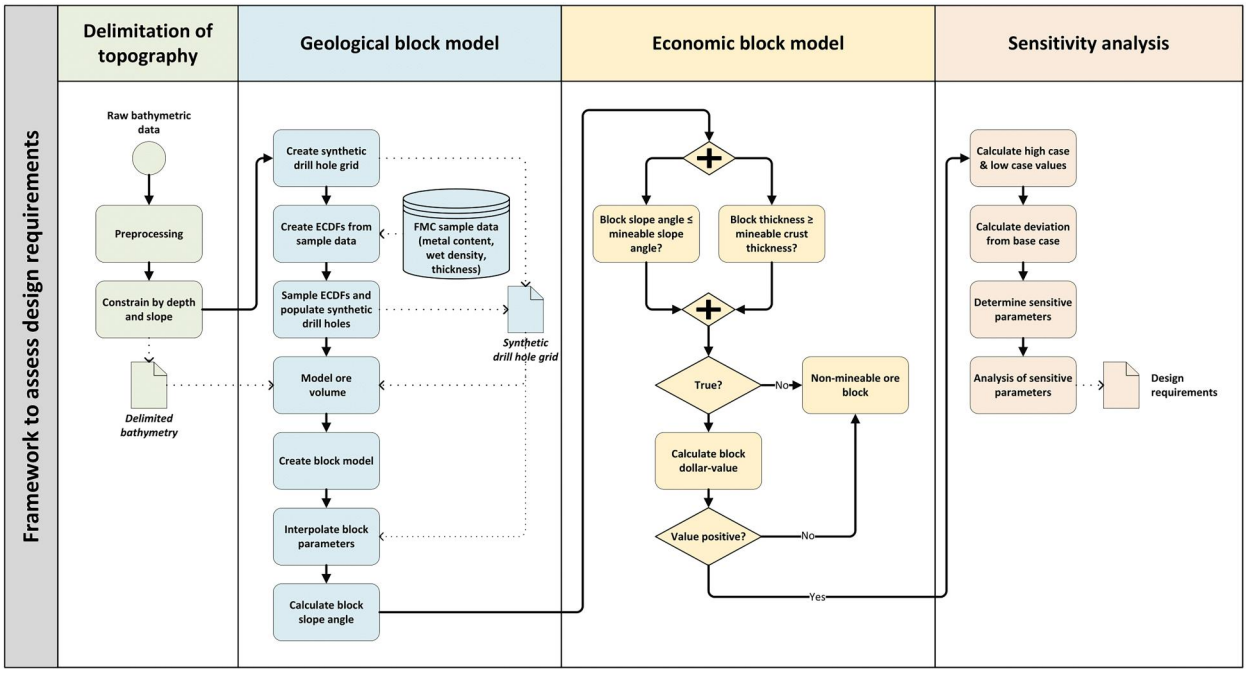

Figure A2. Framework for this study; the methodological workflow illustrates the key steps and processes involved in the analysis.

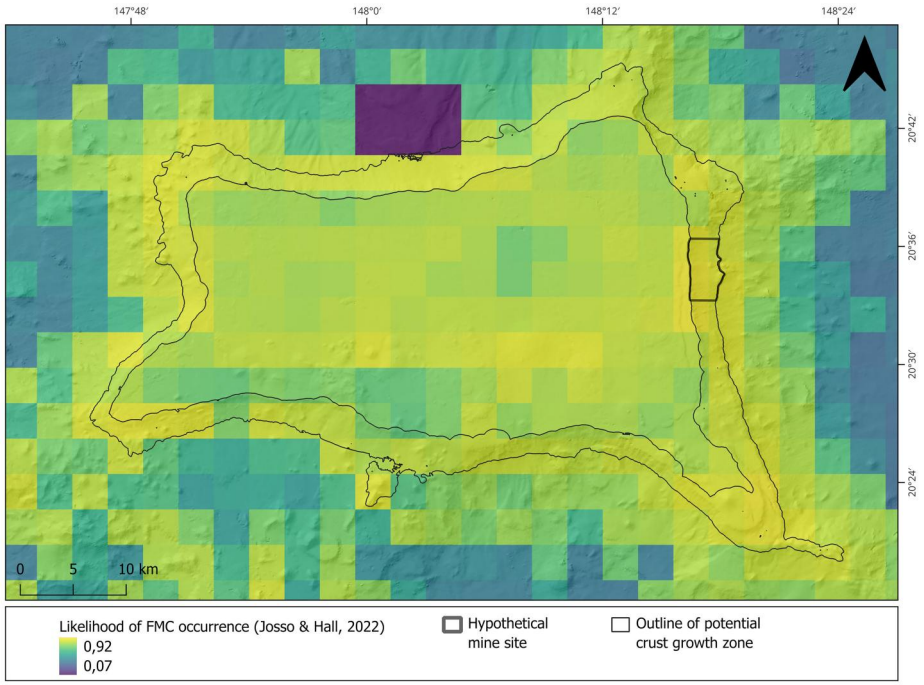

Figure A3. Overlay of potential crust growth zone and hypothetical mine site at Fryer Guyot on a crust prospectivity map, derived from data provided by Josso and Hall (2022).

Table A1. Summary statistics of FMC samples from four Magellan Seamount guyots (values rounded to zero decimals).

Min. thickness (cm)	Max. thickness (cm)	Mean thickness (cm)	Standard deviation (cm)	Mean water depth (m)	*N*	References
1	24	10	5	1928	132	Du (2020)

The empirical cumulative distribution function (ECDF) was computed from the full-precision dataset.

Table A2. Statistical parameters (rounded for display) for a subset of FMC samples extracted from Adamczyk et al. (2023)'s dataset.

Metal	Minimum (ppm)	Maximum (ppm)	Mean (ppm)	Median (ppm)	Standard deviation (ppm)	*N*	References
Cu	40	2805	575	426	456	263	Adamczyk et al. (2023)
Ni	21	8565	2766	2431	1702	264	Adamczyk et al. (2023)
Co	9	13,173	4092	3458	2692	264	Adamczyk et al. (2023)
Mn	26,400	477,000	209,348	211,000	68,901	266	Adamczyk et al. (2023)

The full-precision subset was used to compute ECDFs. It includes samples from water depths between 1500 and 2500 m, corresponding to the FMC growth zone relevant to the hypothetical mine site. These samples have not been genetically classified and likely represent a mix of FMC types.

Table A3. Physical properties of FMC and substrate based on various literature sources (rounded for display).

Physical property	Unit	Arithmetic mean	*N*	Location	References
Mean wet bulk density ($\rho_{\text{crust, wet}}$)	g/cm^3	2	31	Necker Ridge, Karin Ridge	Hein et al. (1985); Sviniinnikov (1994)
Mean water content crust ($\text{water}_{\text{crust}}$)	% wt.	32	13	Necker Ridge	Hein et al. (1985)
Mean water content substrate ($\text{water}_{\text{substrate}}$)	% wt.	21	10	Necker Ridge, Horizon Guyot, S.P. Lee Guyot	Hein et al. (1985)

Mean water contents are assumed to represent both saturation and sorbed water. The wet bulk density dataset was used to compute ECDFs.

Table A4. Overview of the selected metallurgical processing route: FMC and substrate recoveries (beneficiation) and metal recoveries (extractive metallurgy).

Process	Beneficiation	Extractive metallurgy	References
Type	Gravity separation by jig	RKEF smelting and sulfuric acid leaching	Section 2.2, Figure A1
Crust recovery ($\eta_{\textbf{beneficiation}, crust}$)	90%	–	Morgan (2006)
Substrate recovery ($\eta_{\textbf{beneficiation}, substrate}$)	10%	–	Morgan (2006)
Cu recovery ($\eta_{\textbf{metallurgy}, \text{Cu}}$)	–	86%	AMC (2021)
Ni recovery ($\eta_{\textbf{metallurgy}, \text{Ni}}$)	–	95%	AMC (2021)
Co recovery ($\eta_{\textbf{metallurgy}, \text{Co}}$)	–	77%	AMC (2021)
Mn recovery ($\eta_{\textbf{metallurgy}, \text{Mn}}$)	–	99%	AMC (2021)
Products	–	Cu cathodes, Co sulfate, Ni sulfate, Mn silicate	AMC (2021)

Table A5. Overview of metal content and commodity prices for metallurgical products of the selected processing route.

Metallurgical product (*i*)	Metal content ($g_{\text{product}, i}$)	Estimated product price ($\text{price}_{\text{product}, i}$)
Cu cathodes	100%	8237 USD/t
Ni sulfate	22%	4687 USD/t
Co sulfate	21%	8385 USD/t
Mn Silicate	40%	230 USD/t

Metal content is from AMC (2021). All product prices in USD per dry ton. All figures are rounded to the nearest whole number.

Table A6. Inflation-adjusted commodity prices (in USD per dry ton).

	Cu cathodes (99.9% Cu)		Ni sulfate (22% Ni)		Co sulfate (20.5% Co)		Mn silicate (40% Mn)	
Year	Price (USD/t)	PPI factor	Price (USD/t)	PPI factor	Price (USD/t)	PPI factor	Price (USD/t)	PPI factor
2014	8813.09	1.27	4524.64	1.25	9732.61	1.25	228.72	1.71
2015	8162.90	1.42	4305.59	1.25	8283.61	1.25	219.07	1.97
2016	7031.64	1.45	3253.93	1.36	7781.41	1.36	187.28	2.05
2017	7965.89	1.30	3688.98	1.35	11051.65	1.35	324.62	1.74
2018	8257.74	1.25	4497.45	1.26	6340.18	1.26	316.40	1.63
2019	7957.14	1.32	4903.84	1.23	9404.83	1.23	326.76	1.49
2020	7689.28	1.27	4641.30	1.25	9611.75	1.25	202.73	1.22
2021	9201.36	0.99	5370.74	1.17	9470.63	1.17	160.89	1.05
2022	8636.32	0.95	6307.09	1.02	4765.43	1.02	167.78	0.99
2023	8657.89	1.00	5372.27	1.00	7412.02	1.00	167.29	1.00
Average	8237.33	–	4686.58	–	8385.41	–	230.15	–

For each commodity and year, the inflation-adjusted values were calculated by multiplying the nominal prices by the ratio of the producer price Index (PPI) for the specific year to the PPI index for 2023. Nominal prices were estimated from U.S. International trade commission import data. The PPI factors were calculated using commodity-specific indices reported by the U.S. Bureau of labor statistics. When a specific index was unavailable, the next higher level of aggregation was used to calculate the PPI factors, as suggested by Sager (personal communication, July 29, 2024). Manganese silicate was priced based on import data for 20–47% manganese ores, due to its comparable quality (Boulby, Canaguier, and Donald 2023).

Table A7. Different efficiency factors along the value chain for an FMC mining operation informed by SMS and PMN mining.

FMC efficiency factors	Value (%)	Deposit type	References
FMC excavation efficiency ($\eta_{\mathbf{excavation}}$)	90	SMS	SRK Consulting (2010)
FMC collection efficiency ($\eta_{\mathbf{collection}}$)	90	SMS	SRK Consulting (2010)
FMC transport efficiency ($\eta_{\mathbf{transport}}$)	93	PMN	AMC (2021)
Base case mining efficiency ($\eta_{\mathbf{mining,\,block}}$)	75	–	Equation (5) of this article

Table A8. Proposed mining rates for various FMC mining scenarios.

Study site	Production rate per annum (kt, dry)	Production rate per annum (kt, wet)	References
Johnston Island	700	920*	Morgan (2006)
Marshall Islands	1000	1320*	Callies and Johnson (1989)
Broder Pacific Prime Crust Zone	–	910	Goto et al. (2009)
Marshall Islands	670	890*	SPC (2016)
Broader Pacific Prime Crust Zone	–	1000	Hein, Conrad, and Dunham (2009)
Base case, this study (mining $\mathrm{rate}_{\mathbf{nominal,\,period}}$)	680*	1000	–

Mining rates marked with an * were recalculated assuming the mean crust water content stated in Table A3 (32%). Base-case values are the arithmetic mean of the production rates across all scenarios. Values are rounded for display.

Table A9. Base case operating cost per ton and per day.

Study site	Production rate per annum (kt, dry)	Cost per ton (USD, dry)	Daily cost (USD, asset $\mathrm{cost}_{\mathbf{time}}$)
Solwara-1	1350	90	331,064
Base case	680	90	165,770

Solwara-1's per-ton cost (SRK Consulting 2010) was updated to 2023 dollars using the U.S. Bureau of labor statistics' consumer price Index, then used to derive the base case values. Daily costs are assumed to include expenses related to seafloor mining tools, the lifting system, surface support vessel, and transport barges. All figures are rounded to the nearest whole number.

Table A10. Operational expenditure for the selected processing routes.

Process	OPEX	References
Beneficiation ($\mathrm{Cost}_{\mathrm{beneficiation,\,ton}}$)	8 USD/wet t	EQR (2023)
Extractive metallurgy ($\mathrm{Cost}_{\mathrm{metallurgy,\,ton}}$)	136 USD/dry t	AMC (2021)

Beneficiation costs are based on 2023 figures from an onshore mining project, converted from AUD to USD at an exchange rate of 0.68 without inflation adjustments. Although derived from a 0.4 million ton per year jig circuit, these costs are assumed applicable to the 1 million ton per year base case through economies of scale. Metallurgical processing costs reflect TMC's forecasted average onshore cost during steady-state production. Costs are assumed to cover all onshore costs, including ore transportation, reagent consumption, and energy use. All figures are rounded to the nearest whole number.

Table A11. Parameters for the RBF interpolant in Leapfrog Geo (using block model 30 as an example).

Attribute	Co	Cu	Ni	Mn	Wet density	Crust thickness
Interpolant	Spheroidal	Spheroidal	Spheroidal	Spheroidal	Spheroidal	Spheroidal
Total sill (variance)	7,090,000 ppm^2	219,000 ppm^2	3,060,000 ppm^2	4,080,000,000 ppm^2	0.0267 $\left(\frac{\mathrm{t}}{\mathrm{m}^3}\right)^2$	0.00317 m^2
Base range	500 m	500 m	500 m	500 m	500 m	500 m
Drift	Constant	Constant	Constant	Constant	Constant	Constant
Alpha	3	3	3	3	3	3
Nugget	709,000 ppm^2	21,900 ppm^2	306,000 ppm^2	408,000,000 ppm^2	0.001335 $\left(\frac{\mathrm{t}}{\mathrm{m}^3}\right)^2$	0.0001585 m^2

Following Barnes (1991), the variogram sill was estimated from the sample variance. Thus, the sill was set equal to the sample variance. The base range was set to 500 m (twice the drill hole spacing in planar view) to reflect a common multiple of the sampling distance. The nugget effect was defined as 10% of the sill for metal grades (reflecting higher assumed variability) and 5% for FMC thickness and wet density (reflecting more reliable measurements). A spheroidal interpolant was chosen to model the decay in spatial correlation with distance.